CFD Letters

Journal homepage:
https://semarakilmu.com.my/journals/index.php/CFD_Letters/index
ISSN: 2180-1363

Thermophoresis, Brownian Diffusion, Porosity, and Magnetic Parameters' Effects on Three-Dimensional Rotating Ag-CuO/H_2O Hybrid Nanofluid Flow across a Linearly Stretched Sheet with Aligned Magnetic Field

Abdur Raheem Mohammed[1], Mohiddin Shaw Shaik[2,*], Mohana Ramana Ravuri[2], Maheswari Chundru[2], Dharmaiah Gurram[2]

[1] GR Department, UTAS-SOHAR, Sultanate of Oman, Oman
[2] Department of Mathematics, Narasaraopeta Engineering College (Autonomous), Narasaraopet, A.P., India

ARTICLE INFO

Article history:
Received 24 April 2023
Received in revised form 20 May 2023
Accepted 21 June 2023
Available online 1 October 2023

Keywords:
Hybrid Nanofluid; Thermophoresis; Brownian Diffusion; Forchheimer Number; Aligned Magnetic Field

ABSTRACT

Nanofluids are crucial to explore since they have substantial industrial applications and their rapid heat transfer rates. A brand-new category of nanofluid called "hybrid nanofluid" is now being employed to speed up heat transfer even further. The objective and novelty of this study investigates the impact of different parameters on the flow of a rotating, three-dimensional Ag-CuO/H_2O hybrid nanofluid over a linearly stretched sheet with an aligned magnetic field. These parameters include thermophoresis, Brownian diffusion, porosity, magnetic parameter, and Forchheimer number. The study revealed that when temperatures decrease, CuO and Ag nanoparticle volume fractions lead to improved concentration and velocity profiles, correspondingly, momentum and concentration boundary layer thickness are enhanced while thermal boundary layer thickness is reduced. The investigation also reveals that while temperature rises with higher levels of some parameters, the velocity profile and concentration fall, correspondingly, momentum and concetration boundary layer thickness are reduced. The effects of different factors on the rates of skin friction, heat, and mass transmission can also be explored. Higher values of K and cause the Nusselt and Sherwood numbers to rise, whereas $Fr, \epsilon, \mathrm{M}, \alpha$ and Nb cause them to fall. The nonlinear ODEs formed from the governing system of nonlinear PDEs are solved in the study using MATLAB and the BVP-5C shooting method. The contribution of this work is to the understanding of the behaviour of hybrid nanofluids and its potential applications in the development and optimization of nanofluid-based systems for various engineering applications.

1. Introduction

A hybrid nanofluid is a type of fluid that contains a variety of one or more different kinds of nanoparticles that are smaller than 100 nanometres in size. Base fluids like water, oil, biological fluids, and metals, oxides, and carbon-based compounds are frequently used in hybrid nanofluids. Hybrid nanofluids outperform conventional nanofluids in terms of heat transfer efficiency helps to their

* *Corresponding author.*
E-mail address: mohiddinshaw@gmail.com (Mohiddin Shaw Shaik)

https://doi.org/10.37934/cfdl.15.10.123151

improved thermal conductivity and stability. Hybrid nanofluids have a variety of potential uses, including cooling electronic devices, lubricating mechanical systems, transferring heat in power plants, acting as coolants in manufacturing, in preparation of madiciens of cancer treatments they acting as catalysts moreover they play crucial role in various chemical reactions, treating wastewater, reducing pollution, and purifying the air.

Numerous researchers investigated the hybrid nanofluid flows in various configurations. In particular industrial segments, research on hybrid nanofluid flows across a linearly stretched regime is crucial. The effectiveness of heat transfer is a crucial aspect in industrial operations, and studying fluid flow over a linearly stretched regime offers insights into how to maximise heat transfer effectiveness. A few of its fascinating applications are the extrusion of plastic sheets for aerodynamic purposes, the manufacture of stretchable polymer materials using the melt spinning technique, the creation of emollients, paints, and glass fibre, among others. Crane [1] conducted initial research on extended hybrid nanofluid flow. Since then, a number of scientists have investigated hybrid nanofluid flows containing different nanoparticles over a stretching sheet. References from previous studies [2-6] explored how 2D/3D rotating hybrid nanofluid flows across a linearly expanding zone were affected by chemical reaction, heat generation, radiation, velocity slip, nanoparticle volume friction, and convective conditions.

In an MHD fluid flow, the relationship between the magnetic regime and the velocity of an electrically conducting liquid can be investigated. The Lorentz force, which alters the magnetic field, arises when a current passes through a magnetic field. The ratio of electromagnetic to inertial forces provides an indication of the magnetic field's influence on the flow, both in the direction of flow and perpendicular to it. In recent years, there has been a growing emphasis on studying magneto hydrodynamic natural convection heat transfer and fluid flow over porous three-dimensional stretching sheets, particularly with the incorporation of hybrid nanoparticles into the base fluid. This area of research holds significance due to the potential for controlling heat transfer in various energy systems. The utilization of hybrid nanofluids in thermal systems under the influence of an external magnetic field is a rising trend in this field. MHD (magneto hydrodynamic) fluid flows refer to the behaviour of electrically conducting liquids or plasmas when subjected to a magnetic field. These flows are of interest in a wide range of technical and industrial applications, including materials processing, energy conversion, and nuclear fusion research. In particular, MHD flows can be used to control fluid movement and heat transfer in various systems, such as the stretching of plastic sheets, metal casting, crystal growth, and cooling liquid metal blankets. They can also be employed in the design of tuneable optical fabric filters, optical grafting, and fusion reactors.

MHD hybrid nanoliquid flows through a permeable stretching/shrinking regime about radiation influence is taken from the previous study [7-13]. The use of hybrid nanofluids in flow across porous media has shown significant advantages in the fields of thermal technology, geothermal energy restoration, crude oil extraction, thermal energy storage, thermal insulation, ceramic engineering, groundwater hydrology, and flow over filtering tools, among others. In order to study chemical reaction and radiation, are taken from the previous study [14, 15] investigated the (MHD) hybrid nanoliquid flows via porous media, on stretching sheet.

A dimensionless parameter known as the Forchheimer number is used to characterise the resistance flow of liquid in a porous medium. A hybrid nanofluid considers the effects of both suspended nanoparticles and porous surfaces. It is used to optimise the design of porous structures and nanofluid formulations for a variety of uses, including filtration, energy conversion, and thermal management. It is a crucial parameter in studies of heat transfer and flow through porous media. Forchheimer number impact on hybrid nanoliquid flows in a permeable media through stretching sheet was proposed by Saeed *et al.,* [16] and Usman *et al.,* [17]. Lateral many researchers spend

their concentration on Forchheimer in different environment are taken from the previous study [18-20].

In hybrid nanofluids, an essential property that defines the degree of alignment of magnetic particles in a magnetic field is known as an aligned magnetic parameter. Energy storage, heat transfer, and biomedical engineering all have potential uses. Khan, Ayub, Soumini dolui and khan *et al.,* [21] reported aligned magnetic regime influence on hybrid nano liquid on a linearly stretched region.

Brownian motion and thermophoresis diffusion are two significant physical processes that have an impact on the behaviour of a mixed nanofluid. Hybrid nanofluids' distinctive thermal characteristics, which are influenced by thermophoresis diffusion and Brownian motion, make them appealing for a variety of industrial uses, including solar collectors, automotive radiators, and electronics cooling. Many biomedical uses, including targeted drug delivery and hyperthermia cancer therapy, are being investigated for hybrid nanofluids. While thermophoresis allows for the precise control of nanoparticle concentration and localization in particular areas of the body, Brownian motion can assist in dispersing nanoparticles uniformly throughout the fluid. In spacecraft thermal management systems, where the capacity to dissipate surplus heat is crucial to maintaining the safety and functionality of the spacecraft, hybrid nanofluids are being explored for use in spacecraft propulsion systems. The fluid in these systems can have its heat transfer characteristics optimised by Brownian motion and thermophoresis. Due to the lack of numerical research on the heat transfer properties for 3D rotating hybrid nanofluid boundary layer flow over a stretched sheet with rotating, $\mathrm{Ag}-\mathrm{CuO}/\mathrm{H_2O}$ hybrid nanoliquid flow on a linearly stretching surface have not been discussed yet and the current investigation is an attempt address this shortfall. The objective of the current research is to investigate these impacts. The transformed nonlinear ODEs, are solved numerically by using BVP-5C shooting method through MAT lab. The novelty of the work is studying the effects of nanoparticle volume fraction, porosity parameter, Forchheimer number, rotation parameter, wedge parameter, magnetic parameter, aligned magnetic field parameter, chemical reaction parameter, radiation, Brownian, thermophoresis parameter, stretching ratio parameter and Schmidt number on velocity profile along x and y-axes, temperature and concentration segmentations. The skin-friction, Nusselt and Sherwood numbers are given through tables. When compared to the existing literature [22,23], the obtained findings are perceived in high agreement.

2. Mathematical Formulation

In this study, 3-D rotating, $\mathrm{Ag}-\mathrm{CuO}/\mathrm{H_2O}$ hybrid nanoliquid flow past a linearly stretched surface at $z=0$ is considered. Figure 1 depicts problem model flow. Copper Oxide and Silver nano-sized particulates with $\mathrm{H_2O}$ as base fluid, is assumed. CuO nanoparticles with volume fraction ϕ_1 is dispersed keen on the base fluid $\mathrm{H_2O}$ produce $\mathrm{CuO}-\mathrm{H_2O}$ nanofluid. To evolve the destination $\mathrm{Ag}-\mathrm{CuO}/\mathrm{H_2O}$ hybrid nanoliquid silver with volume fraction ϕ_2 is distributed into $\mathrm{CuO}-\mathrm{H_2O}$ nanofluid. The nanofluid rotation is done such that the fluid's angular velocity Ω stays the same when it is rotated around the vertical axis.

With these assumptions, the considered reigning equations are (Hayat and Nadeem [22]):

$$\frac{\partial u}{\partial x}+\frac{\partial v}{\partial y}+\frac{\partial w}{\partial z}=0 \tag{1}$$

$$u\frac{\partial u}{\partial x}+v\frac{\partial u}{\partial y}+w\frac{\partial u}{\partial z}-2\Omega v=\nu_{hnf}\frac{\partial^2 u}{\partial z^2}-\frac{\sigma_{hnf}}{\rho_{hnf}}B_0^2 sin^2\alpha\, u+\frac{\nu_{hnf}}{K^*}u-\frac{C_b}{x\sqrt{K^*}}u^2 \tag{2}$$

$$u\frac{\partial v}{\partial x}+v\frac{\partial v}{\partial y}+w\frac{\partial v}{\partial z}+\ 2\Omega u=\ \nu_{hnf}\frac{\partial^2 v}{\partial z^2}-\frac{\sigma_{hnf}}{\rho_{hnf}}B_0^2 sin^2\alpha\ v+\frac{\nu_{hnf}}{K^*}v-\frac{C_b}{x\sqrt{K^*}}v^2 \tag{3}$$

$$u\frac{\partial T}{\partial x}+v\frac{\partial T}{\partial y}+w\frac{\partial T}{\partial z}$$
$$=\ \alpha_{hnf}\frac{\partial^2 T}{\partial z^2}+\ \frac{Q}{(\rho C_p)_{hnf}}(T-T_\infty)-\frac{1}{(\rho C_p)_{hnf}}\frac{\partial q_r}{\partial z}+\tau\left[\frac{D_T}{T_\infty}\left(\frac{\partial T}{\partial z}\right)^2+D_B\left(\frac{\partial C}{\partial z}\right)\left(\frac{\partial T}{\partial z}\right)\right] \tag{4}$$

$$u\frac{\partial C}{\partial x}+v\frac{\partial C}{\partial y}+w\frac{\partial C}{\partial z}=\ \beta_{hnf}\frac{\partial^2 C}{\partial z^2}-\ \xi_1(C-C_\infty)^n+\frac{D_T}{T_\infty}\left(\frac{\partial^2 T}{\partial z^2}\right) \tag{5}$$

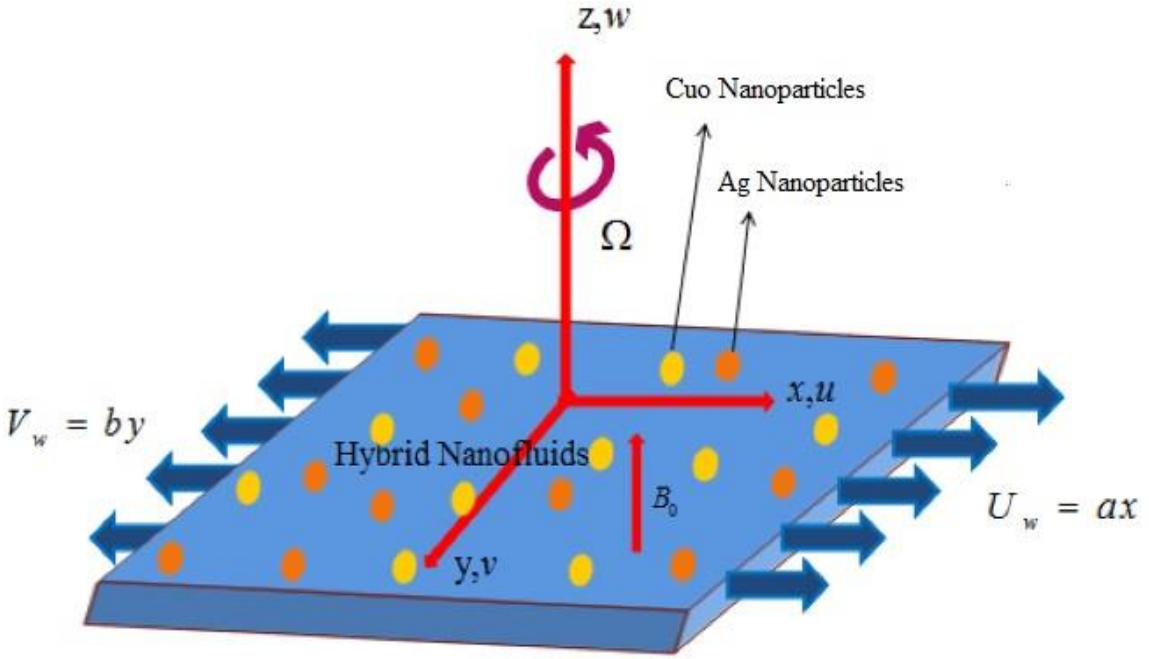

Fig. 1. The flow geometry

According to the above-mentioned assumptions, the provided boundary conditions (Hayat and Nadeem [22]):

$$u=\ U_w=ax, v=\ V_w=by, w=0, T=\ T_w, C=\ C_w\ \ \text{at}\ z=0$$
$$u\ \to 0, v\ \to 0, T\ \to\ T_\infty, C\ \to C_\infty\ \ \text{as}\ z\ \to\infty \tag{6}$$

By Roseland approximation, the radiation flux $q_r=\ \frac{-4\sigma}{3\chi}\frac{\partial T^4}{\partial z}$. By Tailor's series expansion about T_∞, $T^4\approx 4TT_\infty^3-3T_\infty^4$. The similarity transformations are defined as

$$u=axf'(\eta), v=ayg'(\eta), w=\ -\sqrt{a\nu_f}(f(\eta)+g(\eta)), \eta=z\sqrt{\frac{a}{\nu_f}},\ \ \gamma=\frac{y}{x} \tag{7}$$

The aforementioned changes, Eq. (1), applying the aforementioned adjustments Eq. (2) to Eq. (6) converted into the following (Hayat and Nadeem [22]):

$$f''' - (1-\phi_1)^{2.5}(1-\phi_2)^{2.5}\left[(1-\phi_2)\left\{(1-\phi_1)+\phi_1\left(\frac{\rho_{s1}}{\rho_f}\right)\right\}+\phi_2\left(\frac{\rho_{s2}}{\rho_f}\right)\right]\left((1+Fr)f'^2-(f+g)f''-2\epsilon\gamma g'\right)+\left(K-\frac{\sigma_{hnf}}{\sigma_f}(1-\phi_1)^{2.5}(1-\phi_2)^{2.5}Msin^2\alpha\right)f' = 0 \quad (8)$$

$$g''' - (1-\phi_1)^{2.5}(1-\phi_2)^{2.5}\left[(1-\phi_2)\left\{(1-\phi_1)+\phi_1\left(\frac{\rho_{s1}}{\rho_f}\right)\right\}+\phi_2\left(\frac{\rho_{s2}}{\rho_f}\right)\right]\left((1+\gamma\, Fr)g'^2-(f+g)g''+\frac{2\epsilon}{\gamma}f'\right)+\left(K-\frac{\sigma_{hnf}}{\sigma_f}(1-\phi_1)^{2.5}(1-\phi_2)^{2.5}Msin^2\alpha\right)g' = 0 \quad (9)$$

$$\left(\frac{K_{hnf}}{K_f}+\frac{4}{3}R\right)\theta''+Pr\left[(1-\phi_2)\left\{(1-\phi_1)+\phi_1\left(\frac{(\rho C_p)_{s1}}{(\rho C_p)_f}\right)\right\}+\phi_2\left(\frac{(\rho C_p)_{s2}}{(\rho C_p)_f}\right)\right]\left((f+g+N_B\emptyset')\theta'+N_t(\theta')^2\right)+\delta Pr\theta = 0 \quad (10)$$

$$\phi''+\frac{Sc}{(1-\phi_1)(1-\phi_2)}[(f+g)\phi'-Rc\phi]+\frac{1}{(1-\phi_1)(1-\phi_2)}\left(\frac{N_T}{N_B}\right)\left(\frac{Pr}{\left(\frac{K_{hnf}}{K_f}+\frac{4}{3}R\right)}\right)\left[(1-\phi_2)\left\{(1-\phi_1)+\phi_1\left(\frac{(\rho C_p)_{s1}}{(\rho C_p)_f}\right)\right\}+\phi_2\left(\frac{(\rho C_p)_{s2}}{(\rho C_p)_f}\right)\right]\left((f+g+N_B\emptyset')\theta'+N_t(\theta')^2\right)+\delta\left(\frac{Pr}{\left(\frac{K_{hnf}}{K_f}+\frac{4}{3}R\right)}\right)\theta = 0 \quad (11)$$

With boundary conditions,

$$f=0, f'=1, g=0, g'=\lambda, \theta=1, \phi=1 \text{ at } \eta=0$$
$$f'\to 0, g'\to 0, \theta\to 0, \phi\to 0 \text{ as } \eta\to\infty \quad (12)$$

Following are the non-dimensional parameters

$$\nu_{hnf}=\frac{\mu_{hnf}}{\rho_{hnf}},\ \alpha_{hnf}=\frac{K_{hnf}}{(\rho C_p)_{hnf}}, \beta_{hnf}=(1-\phi_1)(1-\phi_2)\beta_f$$
$$\epsilon=\frac{\Omega}{a}, \lambda=\frac{b}{a}, Pr=\frac{\nu_f(\rho C_p)_f}{K_f}, R=\frac{4\sigma T_\infty^3}{\chi K_f}, \delta=\frac{Q}{a(\rho C_p)_f}, Sc=\frac{\nu_f}{\beta_f}, Rc=\frac{\xi_1(C-C_\infty)^{n-1}}{a}$$
$$M=\frac{\sigma_f B_0^2}{a\rho_f}, K=\frac{\nu_f}{aK^*}, Fr=\frac{C_b}{\sqrt{K^*}}, \theta(\eta)=\frac{T-T_\infty}{T_w-T_\infty}, \phi(\eta)=\frac{C-C_\infty}{C_w-C_\infty}.\ ,$$
$$N_t=\frac{D_T\tau(T_w-T_\infty)}{\nu_f T_\infty}\ \ N_b=\frac{D_B\tau(C_w-C_\infty)}{\nu_f} \quad (13)$$

The "Skinfriction" along x and y-axis C_{fx}, C_{fy}, the "local Nusselt number" Nu_x and the "Sherwood number" Sh_x defined by

$$C_{fx} = \frac{\mu_{hnf}\left(\frac{\partial u}{\partial z}\right)_{z=0}}{\rho_f (ax)^2}, C_{fy} = \frac{\mu_{hnf}\left(\frac{\partial v}{\partial z}\right)_{z=0}}{\rho_f (ax)^2}, Nu_x = -\frac{xK_{hnf}}{K_f(T_w - T_\infty)}\left(\frac{\partial T}{\partial z}\right)\Big|_{z=0},$$
$$Sh_x = -\frac{xK_{hnf}}{K_f(C_w - C_\infty)}\left(\frac{\partial C}{\partial z}\right)\Big|_{z=0} \quad (14)$$

(or)

$$Re^{\frac{1}{2}} C_{fx} = \frac{1}{(1-\phi_1)^{2.5}(1-\phi_2)^{2.5}} f''(0)$$
$$\gamma^{-1} Re^{\frac{1}{2}} C_{fy} = \frac{1}{(1-\phi_1)^{2.5}(1-\phi_2)^{2.5}} g''(0)$$
$$Re^{-\frac{1}{2}} Nu_x = -(\frac{K_{hnf}}{K_f} + \frac{4}{3}Rd)\theta'(0),\ Re^{-\frac{1}{2}} Sh_x = -\frac{K_{hnf}}{K_f}\phi'(0) \quad (15)$$

Where $Re = \frac{U_w x}{\nu_f}$ is the restricted Reynolds number.

3. Method of Solution

MATLAB program with "BVP5C" was implemented to solve the Eq. (8) to Eq. (11) along the boundary conditions Eq. (12). In this method $h = 0.01$ was used as the step size and the procedure is continued until the results are accurate to the desired level of precision 10^{-6}. We have discussed the boundary value problems for ordinary differential equations that the bvp5c programme is designed to solve as well as its implementation. For the four-point Lobatto IIIA formula, a striking relationship between scaled residual and real error is discovered. In bvp5c, we take use of this connection to get the control over the real error that is most important to the user while still getting the robustness of a scaled residual control.

4. Results and Discussion

This research article investigates the impact of various parameters on the three-dimensional flow of Ag-CuO/H_2O hybrid nanoliquid past a linearly stretched regime with an aligned magnetic field. Specifically, we study the effect of the Forchheimer number, porosity, Brownian motion, thermophoresis, and magnetic field on the flow. To solve the associated nonlinear ODEs of Eq. (8) to Eq. (11) with boundary conditions given in Eq. (12), we utilized a MATLAB code with the BVP-5C shooting method, which can handle complex BVPs numerically. The obtained results reveal the influence of several parameters, including the volume fraction of nano particulates, rotation, wedge, thermal radiation, Schmidt number, chemical reaction, stretching ratio, and of course the ones mentioned earlier. Tables 1-2. show the physical thermo properties of CuO, Ag nanoparticles and H_2O and $Ag - CuO/H_2O$ hybrid nanofluids respectively. While doing numerical calculations, we consider $n = 0.5$ and $\delta = 0.1$ as default values unless otherwise stated.

Table 1
CuO, Ag and H_2O thermo physical properties [22, 23]

Properties	CuO	Ag	H_2O
ρ	6320	10500	997.1
C_p	531.80	235	4179.0
K	76.50	429	0.6130
Pr	-	-	6.20

Table 2
$Ag - CuO/H_2O$ thermo physical properties [22, 23]

Properties	$\mathbf{Ag - CuO/H_2O}$ **hybrid nanofluid**
Density (ρ)	$\rho_{hnf} = \left[(1-\phi_2)\{(1-\phi_1)\rho_f + \phi_1\rho_{s1}\}\right] + \phi_2\rho_{s2}$
Viscosity (μ)	$\mu_{hnf} = \frac{\mu_f}{(1-\phi_1)^{2.5}(1-\phi_2)^{2.5}}$
Heat Capacity (ρC_p)	$(\rho C_p)_{hnf} = \left[(1-\phi_2)\left\{(1-\phi_1)(\rho C_p)_f + \phi_1(\rho C_p)_{s1}\right\}\right] + \phi_2(\rho C_p)_{s2}$
Thermal Conductivity (K)	$\frac{K_{hnf}}{K_{bf}} = \frac{K_{s2}+(n-1)K_{bf}-(n-1)\phi_2(K_{bf}-K_{s2})}{K_{s2}+(n-1)K_{bf}+\phi_2(K_{bf}-K_{s2})}$ $\frac{K_{bf}}{K_f} = \frac{K_{s1}+(n-1)K_f-(n-1)\phi_1(K_f-K_{s1})}{K_{s1}+(n-1)K_f+\phi_1(K_f-K_{s1})}$
Electrical conductivity (σ)	$\frac{\sigma_{hnf}}{\sigma_{bf}} = \frac{\sigma_{S_2}+2\sigma_{bf}-2\phi_2(\sigma_{bf}-\sigma_{S_2})}{\sigma_{S_2}+2\sigma_{bf}+\phi_2(\sigma_{bf}-\sigma_{S_2})}$ $\frac{\sigma_{bf}}{\sigma_f} = \frac{\sigma_{S_1}+2\sigma_f-2\phi_1(\sigma_f-\sigma_{S_1})}{\sigma_{S_1}+2\sigma_f+\phi_1(\sigma_f-\sigma_{S_1})}$

The impact of the volume fractions of CuO and Ag nanoparticles (ϕ_1 and ϕ_2) on the hybrid nanofluid Ag-CuO/H_2O was analysed using Figures 2-9.

It was observed from the distribution profiles that the concentration and velocity profiles were enhanced, and the temperature decreased as the numerical values of ϕ_1 and ϕ_2 increased. Physically, an increase in volume fraction results in a higher concentration of particles in the fluid, which decreases the density of the Ag-CuO/H_2O hybrid nanofluid. As the density of the fluid decreases for higher values of ϕ_1 and ϕ_2, the enhancement in $f'(\eta)$was observed. The combined effects of increased convection, enhanced thermal conductivity, and increased heat absorption resulted in a decrease in θ(η). As ϕ_1 and ϕ_2 increase, the particle concentration also increases, which leads to a stronger diffusion effect and a decrease in ϕ(η).

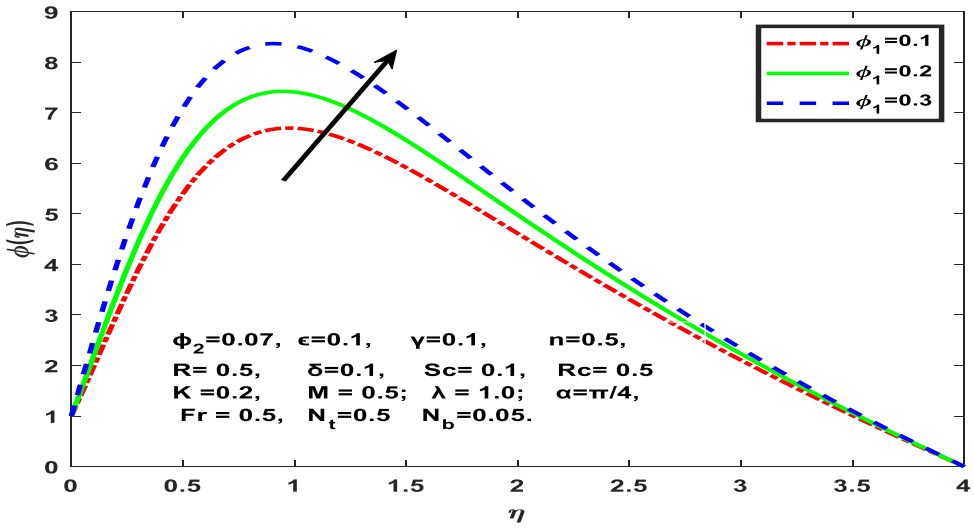

Fig. 2. Consequences of ϕ_1 on concentration Ø

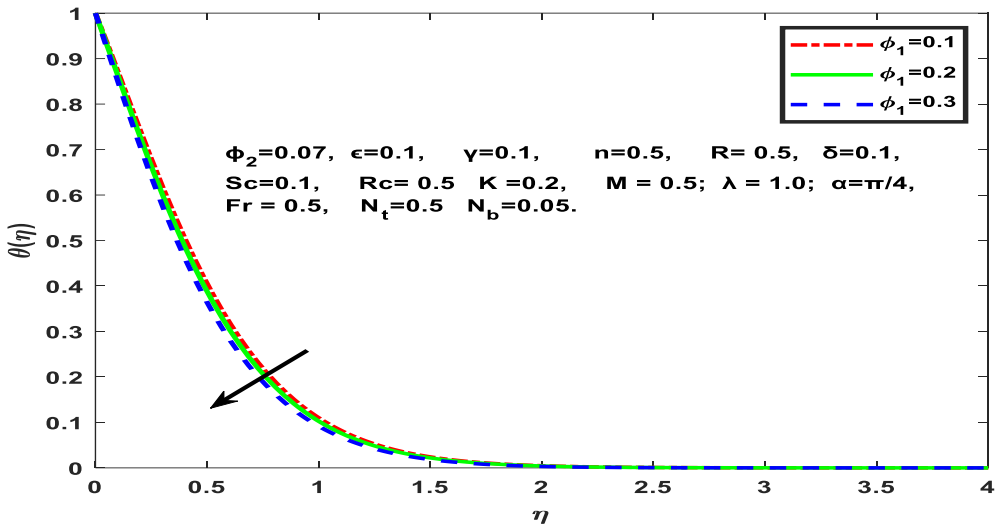

Fig. 3. Consequences of ϕ_1 on Temperature θ

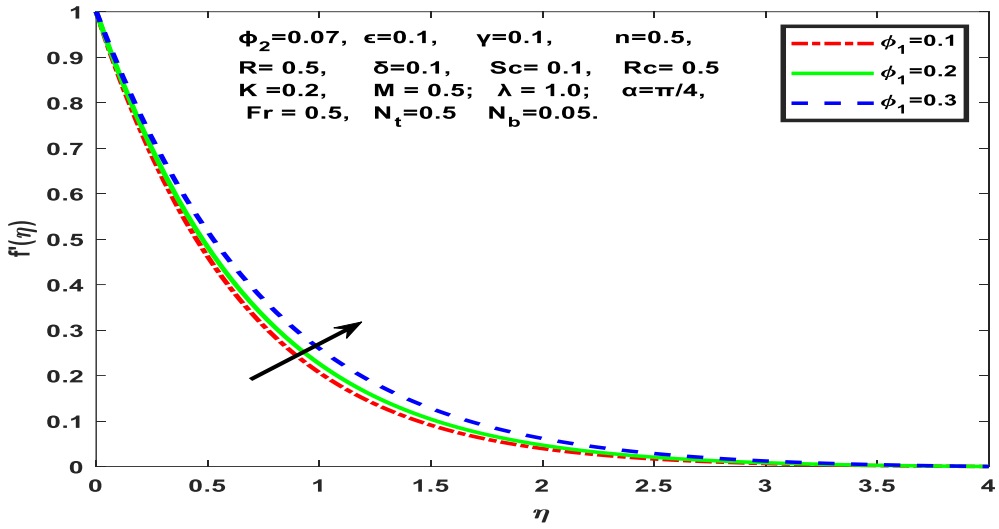

Fig. 4. Consequences of ϕ_1 on Velocity f'

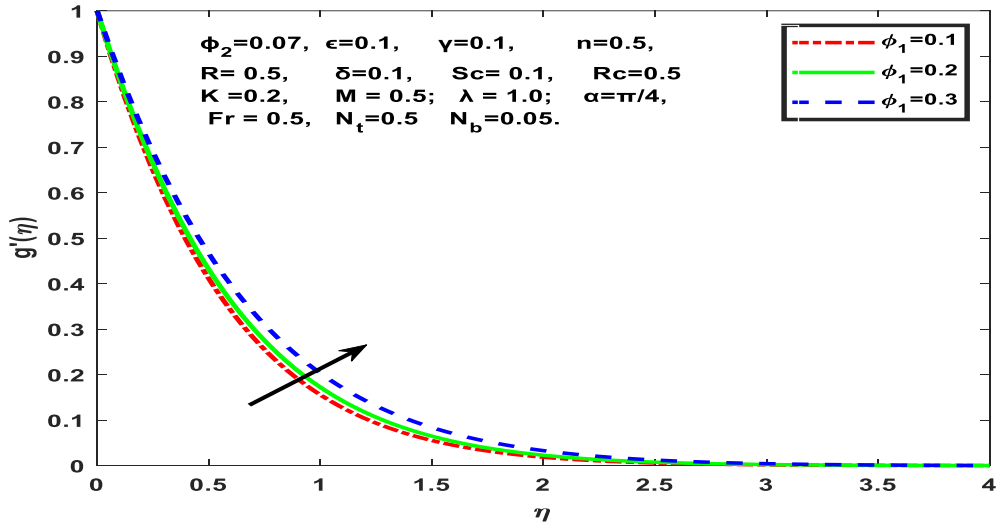

Fig. 5. Consequences of ϕ_1 on Velocity g'

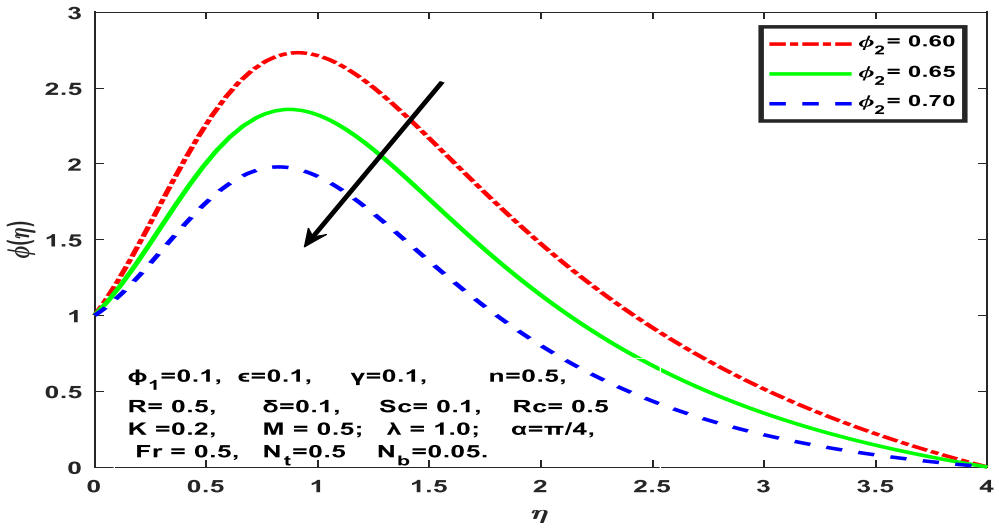

Fig. 6. Consequences of ϕ_2 on concentration $\emptyset$

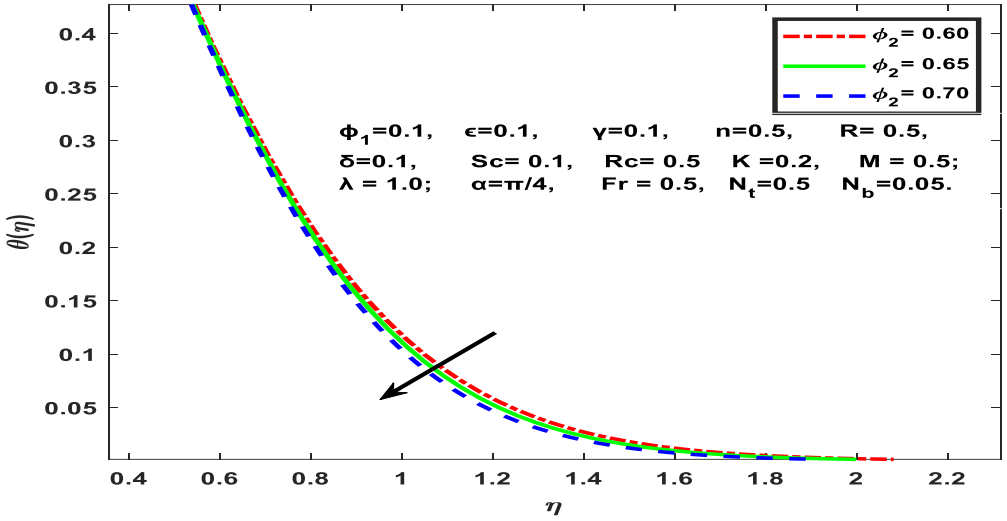

Fig. 7. Consequences of ϕ_2 on Temperature θ

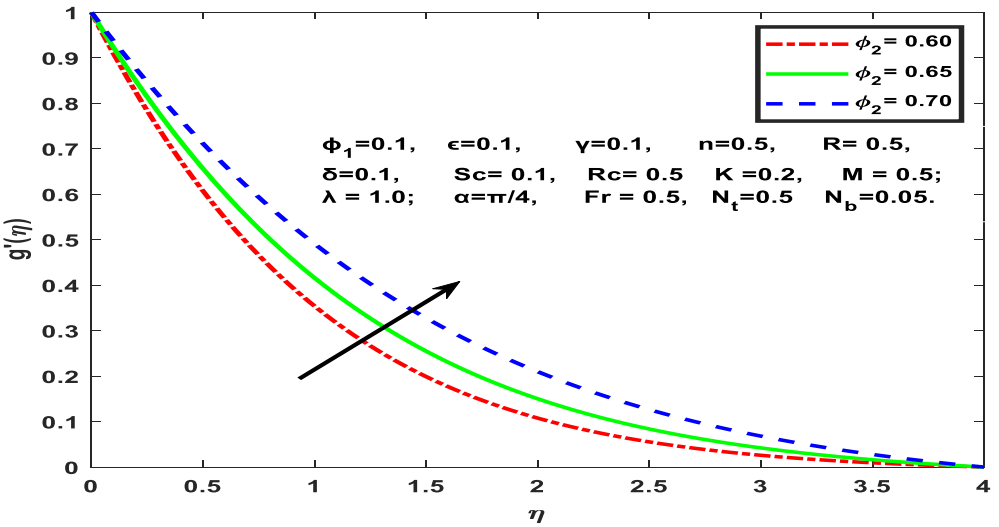

Fig. 8. Consequences of ϕ_2 on Velocity g'

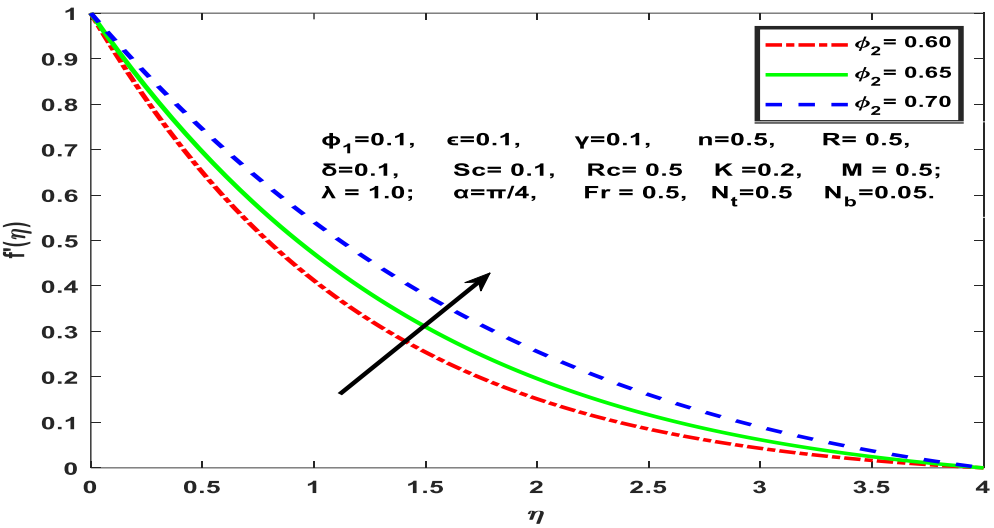

Fig. 9. Consequences of ϕ_2 on Velocityf'

Figures 10-13 portray the impact of rotation parameter ϵ on $f'(\eta)$, $g'(\eta)$, $\theta(\eta)$ and $\phi(\eta)$ for $Ag - CuO/H_2O$ hybrid nanofluid. Greater ϵ leads to decrease in $f'(\eta), g'(\eta)$ and $\phi(\eta)$ an opposite trend observed in $\theta(\eta)$. Physically, due to the combined effects of centrifugal force and shear stress $f'(\eta)$ decreases as ϵ increases. Convective heat transfer, centrifugal force and nanoparticle concentration are increased as ϵ increases, which results in an increment in $\theta(\eta)$. Through centrifugal sedimentation of the particles, the rotation parameter raises the fluid's nanoparticle concentration. This improves the fluid's thermal conductivity and speed up the rate of heat transfer.

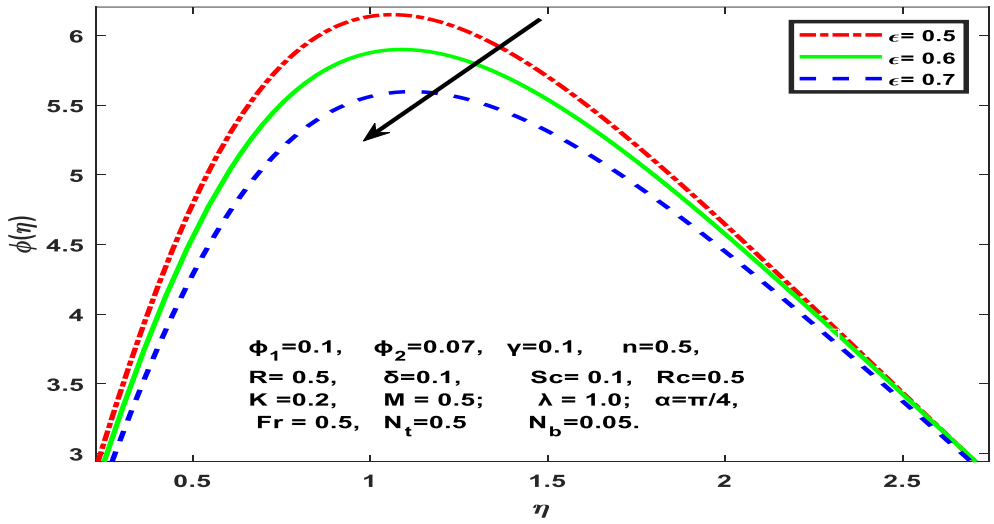

Fig. 10. Consequences of ϵ on concentration $\emptyset$

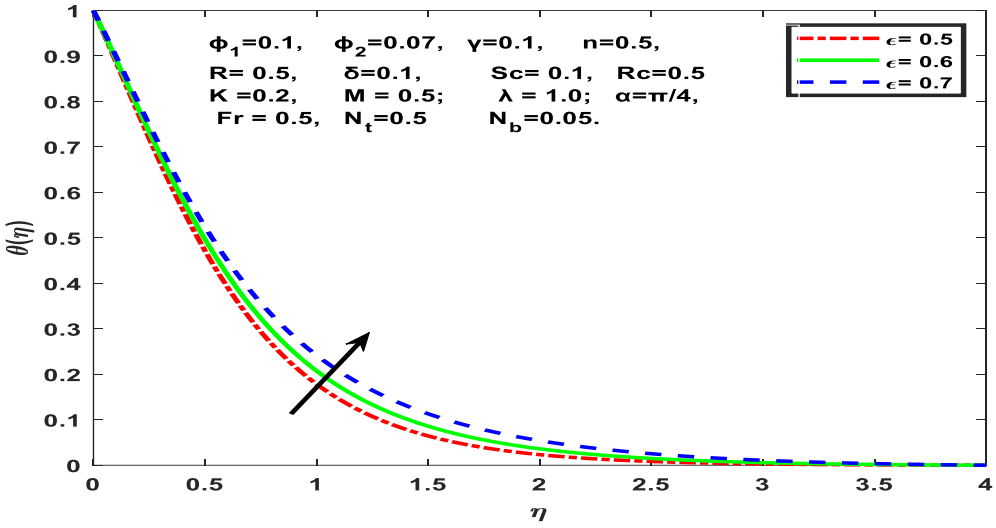

Fig. 11. Consequences of ϵ on Temperature θ

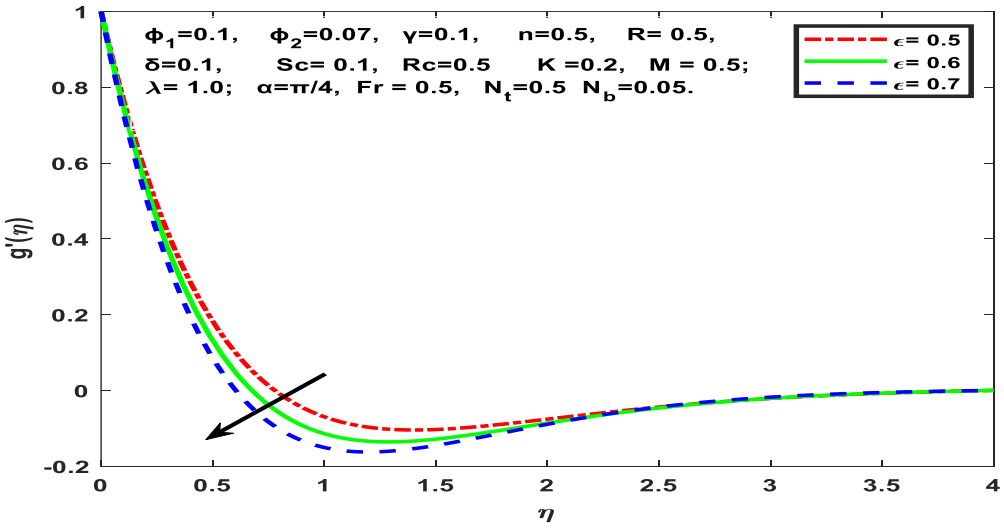

Fig. 12. Consequences of ϵ on Velocity g'

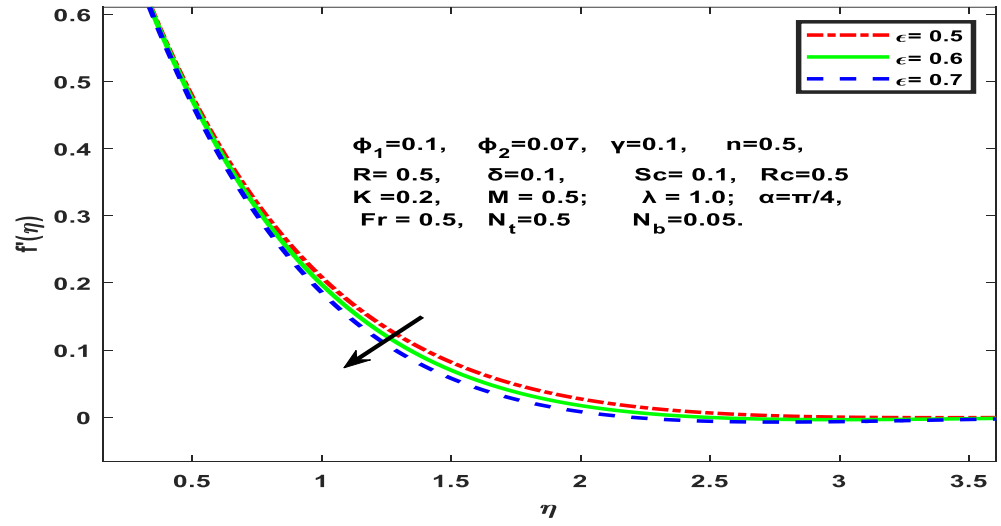

Fig. 13. Consequences of ϵ on Velocity f'

Figures 14-16 show the impact of moving wedge parameter γ on temperature $\theta(\eta)$, $f'(\eta)$ and $g'(\eta)$. Increasing the values of γ decreases the profile of the $f'(\eta)$, $\theta(\eta)$ and enhanced $g'(\eta)$. Physically, increase in γ leads to a steeper angle of the wedge, increased both turbulence and energy in the fluid flow, resulting in an increase in $g'(\eta)$. The physical mechanism of the flow can be used to explain this behaviour. The flow becomes more turbulent and energetic as the wedge angle rises, increasing mixing and, consequently, the fluid's shear stress$g'(\eta)$. At the same time, the increased turbulence and mixing can result in a decrease in the temperature profile $\theta(\eta)$ of the fluid. This is because the mixing causes cooling of the fluid from the outer regions of the flow towards the centre, reducing the temperature gradient across the flow domain.

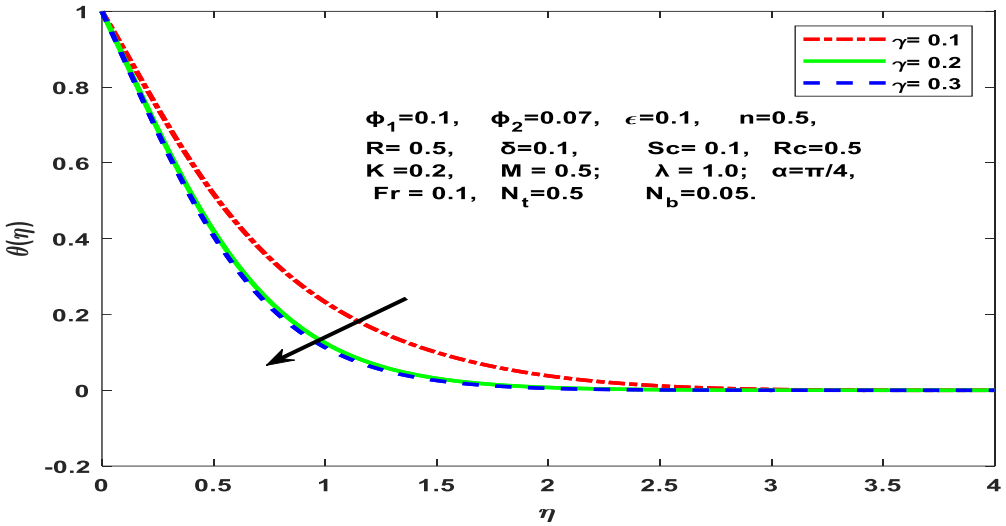

Fig. 14. Consequences of γ on Temperature θ

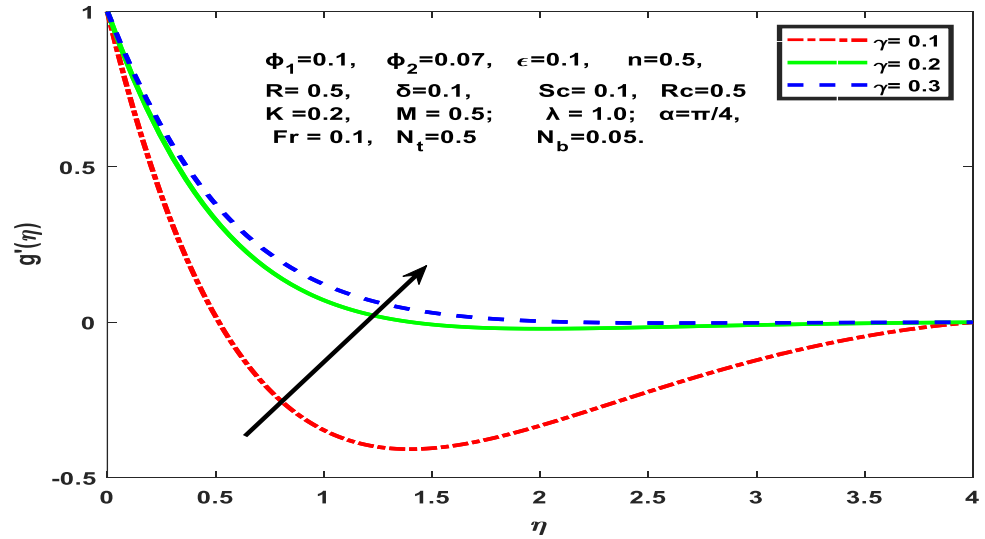

Fig. 15. Consequences of γ on Velocity g'

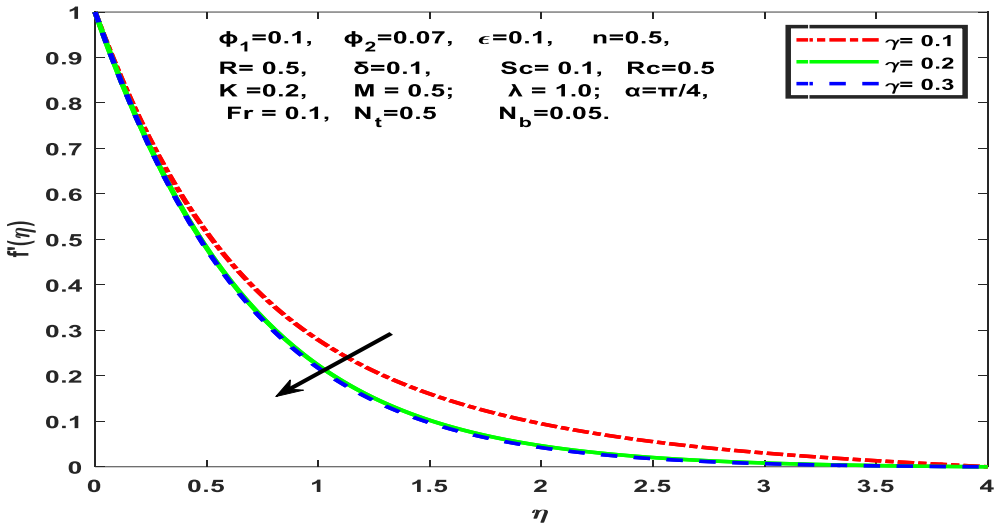

Fig. 16. Consequences of γ on Velocity f'

Figures 17-18 illustrate radiation parameter R influence on concentration and temperature profile $\phi(\eta)$ and $\theta(\eta)$ for $Ag - CuO/H_2O$ hybrid nanofluid. Upsurges in R cause the temperature increments, whereas decrement in the concentration of the fluid. The physical mechanism of the flow can be used to explain this behaviour. The flow becomes more turbulent as the Reynolds number rises, which causes more mixing and, as a result, more heat transfer from the hot surface to the fluid. The temperature may rise as a result of this enhanced heat transfer.

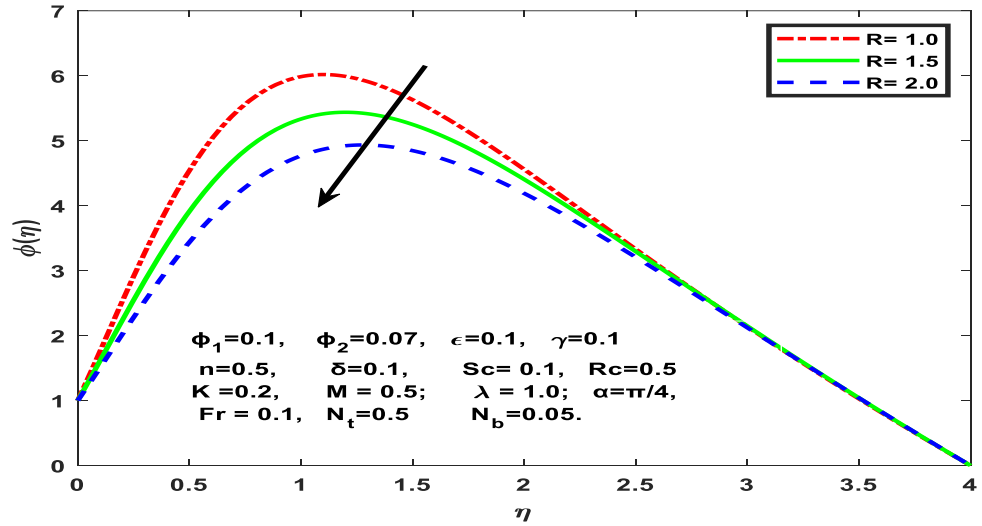

Fig. 17. Consequences of R on concentration Ø

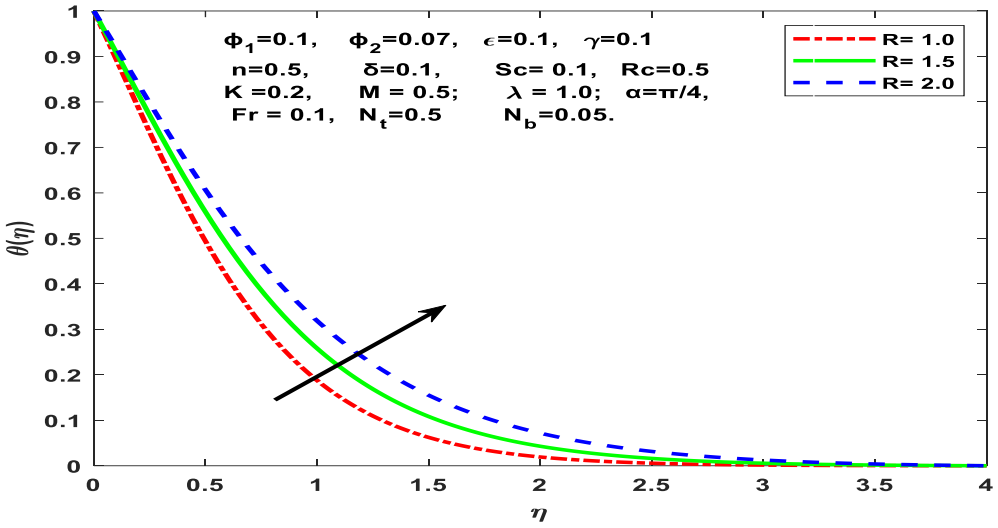

Fig. 18. Consequences of R on Temperature θ

Figure 19 portrays Schmidt number Sc influence on concentration profile $\phi(\eta)$. Since the Schmidt number is the quantitatively related betwixt momentum and mass diffusivity, increasing the values of Sc, the diffusivity falls, the fluid concentration deduces.

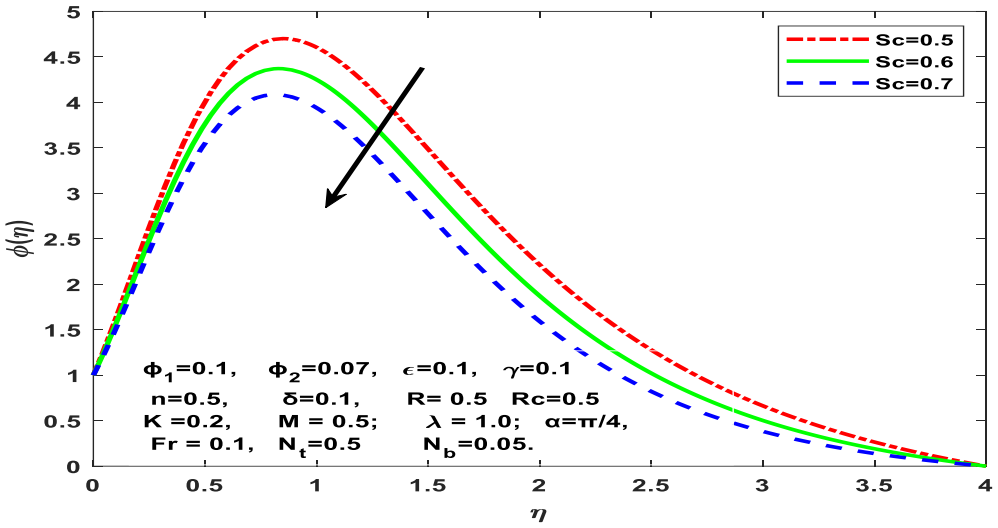

Fig. 19. Consequences of Sc on concentration ∅

Figure 20 shows chemical reaction parameter Rc impact on $\phi(\eta)$. It is noted, $\phi(\eta)$ declines about rising values of Rc. The rate of consumption of the nanomaterials increases as Rc increases, causing a decrease in concentration profile $\phi(\eta)$.

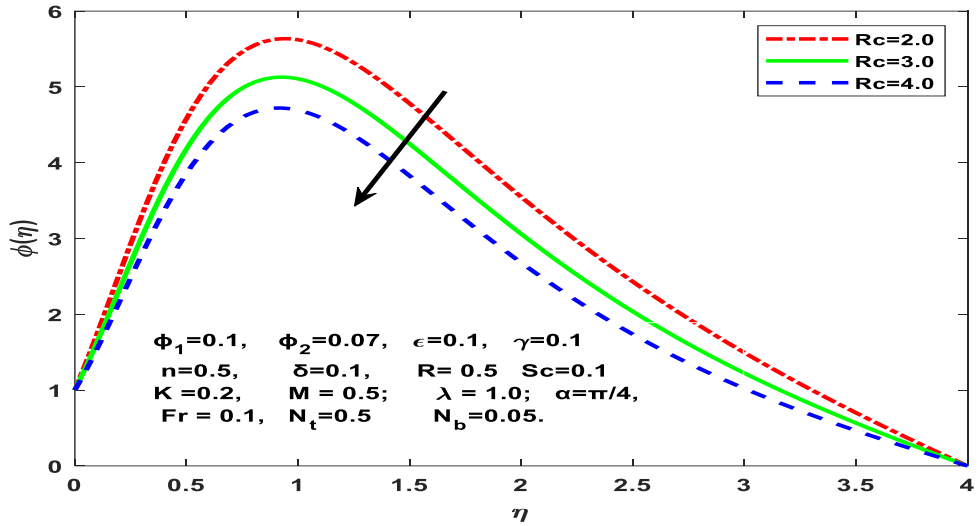

Fig. 20. Consequences of Rc on concentration Ø

From Figure 21, it appears that increasing the value of K leads to a decrease in temperature, with the temperature profile becoming flatter as K increases. This suggests that K associated with a reduction in the heat transfer rate, possibly due to increased fluid viscosity or reduced convective mixing in the fluid.

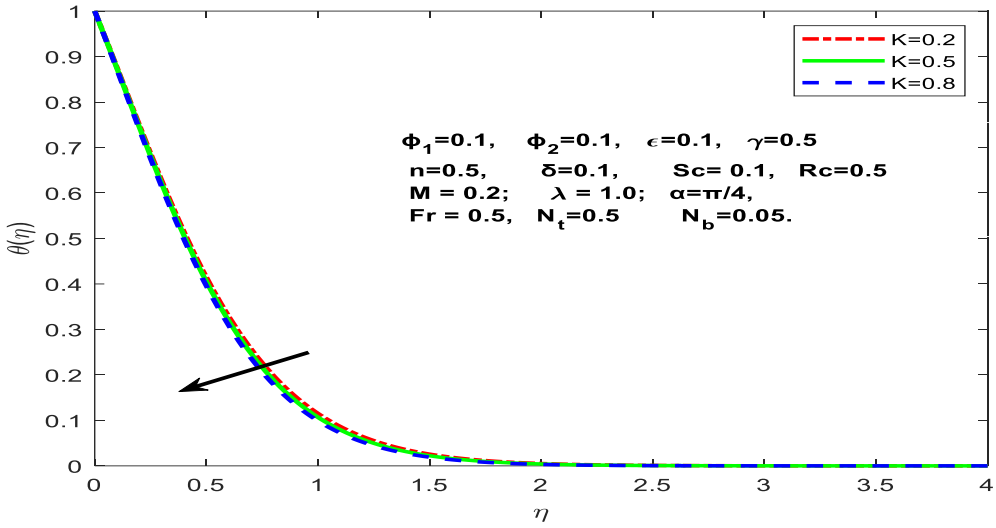

Fig. 21. Consequences of K on Temperature θ

From Figures 22-23, it appears that increasing the value of K leads to an enhancement in the velocity profile of the fluid, with both the$f'(\eta)$and $g'(\eta)$ profiles becoming flatter as K increases.

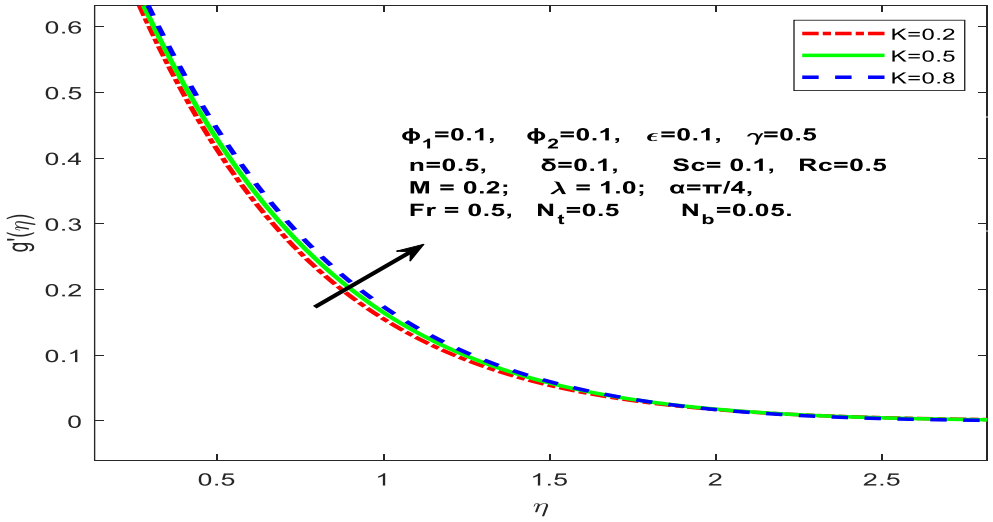

Fig. 22. Consequences of K on Velocity g'

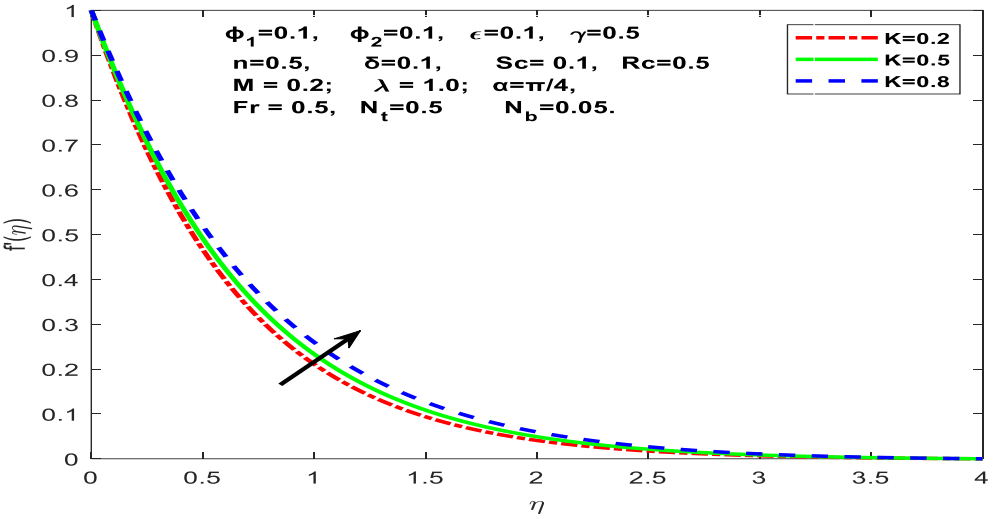

Fig. 23. Consequences of K on Velocity f'

Figures 24-27 demonstrate magnetic parameter M influence on $\phi(\eta)$, $\theta(\eta)$, $f'(\eta)$ and $g'(\eta)$. By strengthening M, $\phi(\eta)$, $f'(\eta)$, $g'(\eta)$ tends to decrease and $\theta(\eta)$ tends to increase. Physically, A drag force analogous to the Lorentz force is generated when a crosswise magnetic regime is applied, which seems to oppose the flow of fluid and hence decrease the$f'(\eta)$. The similar behaviour noted from the references [24-30].

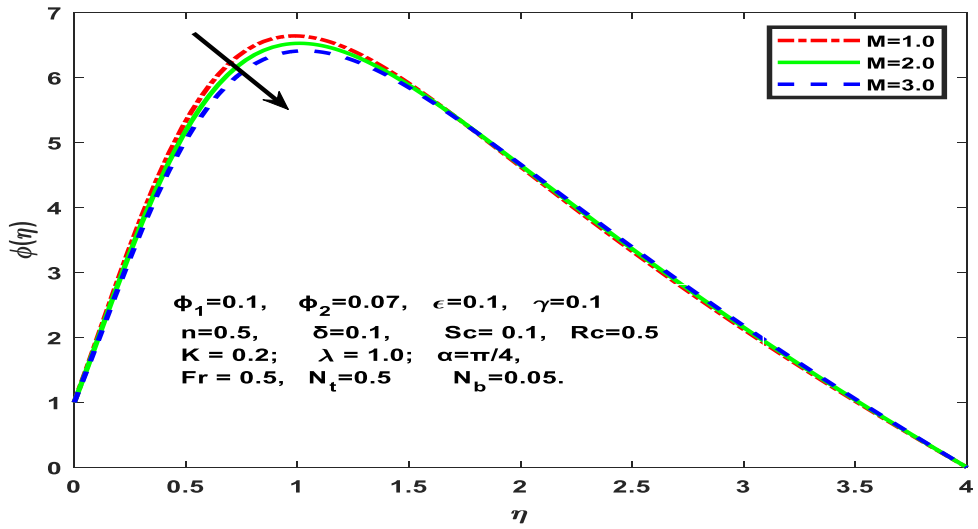

Fig. 24. Consequences of M on concentration ∅

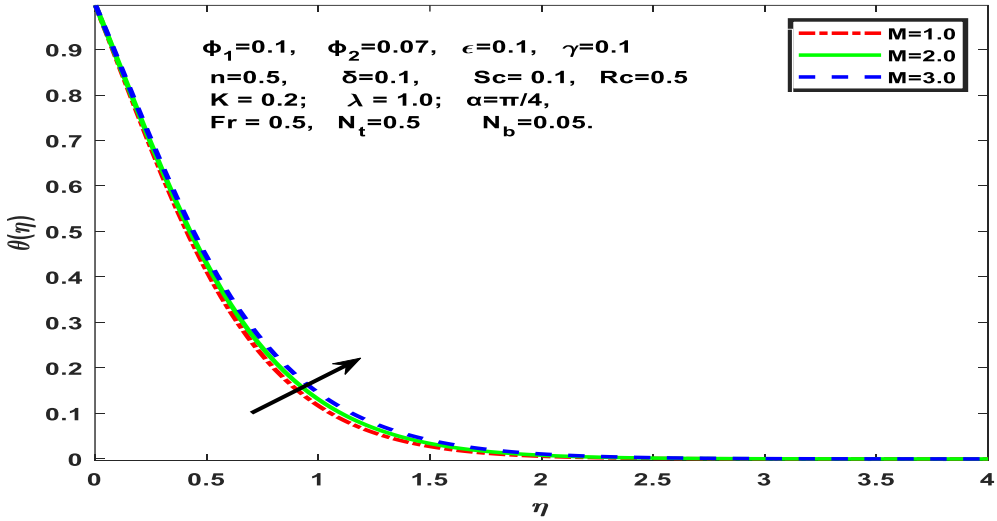

Fig. 25. Consequences of M on Temperature θ

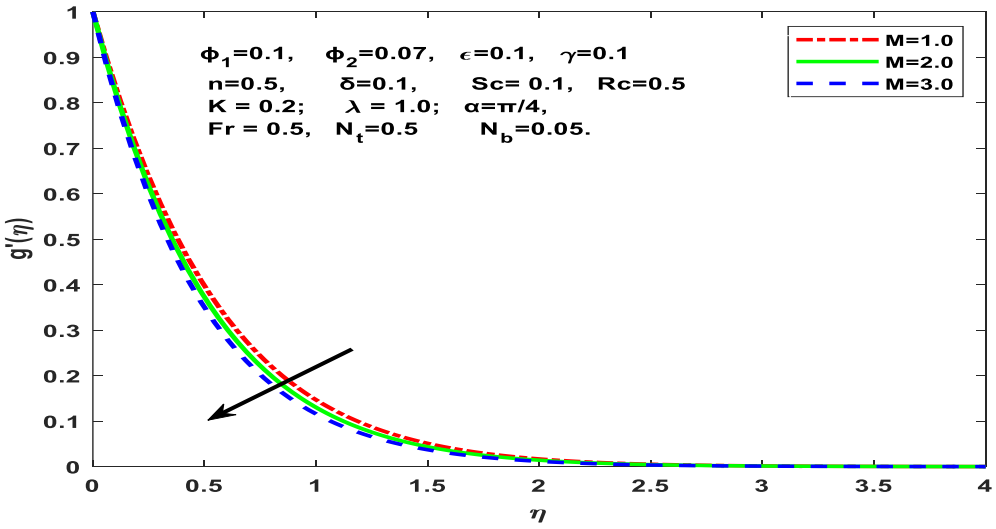

Fig. 26. Consequences of M on Velocity g'

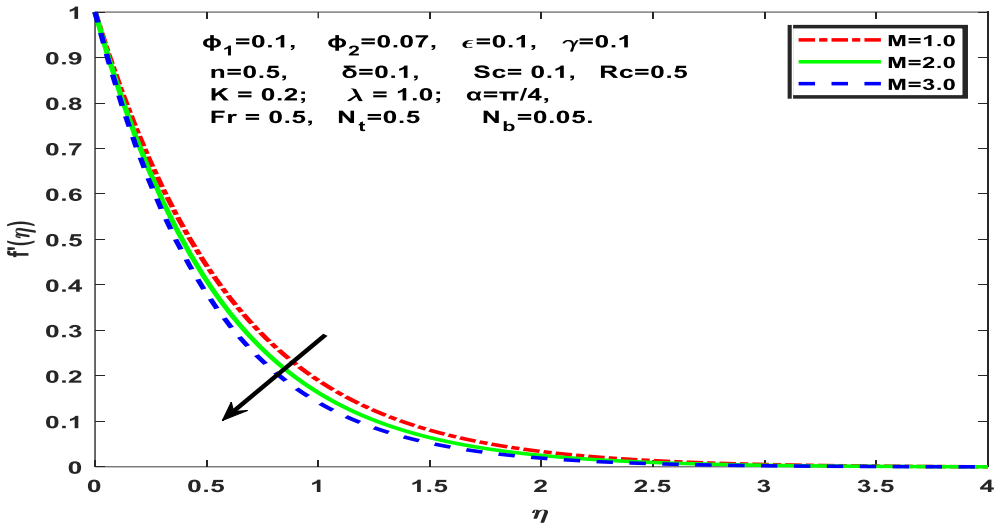

Fig. 27. Consequences of M on Velocity f'

Figures 28-30 demonstrate the stretching ratio parameter λ on $f'(\eta)$, $g'(\eta)$ and $\theta(\eta)$. Increasing the values of λ decreases $f'(\eta)$, $\theta(\eta)$ and $\phi(\eta)$. Reduction in $f'(\eta)$ is owing to an increased resistance to the fluid, the increased stretching. An enhance in λ causes the fluid to stretch faster than it diffuses, leading to a reduction in $\theta(\eta)$ and $\phi(\eta)$. The opposite behaviour is observed in $g'(\eta)$. Physically, the stretching causes the fluid to experience a greater shear force, which leads to an increase in $g'(\eta)$.

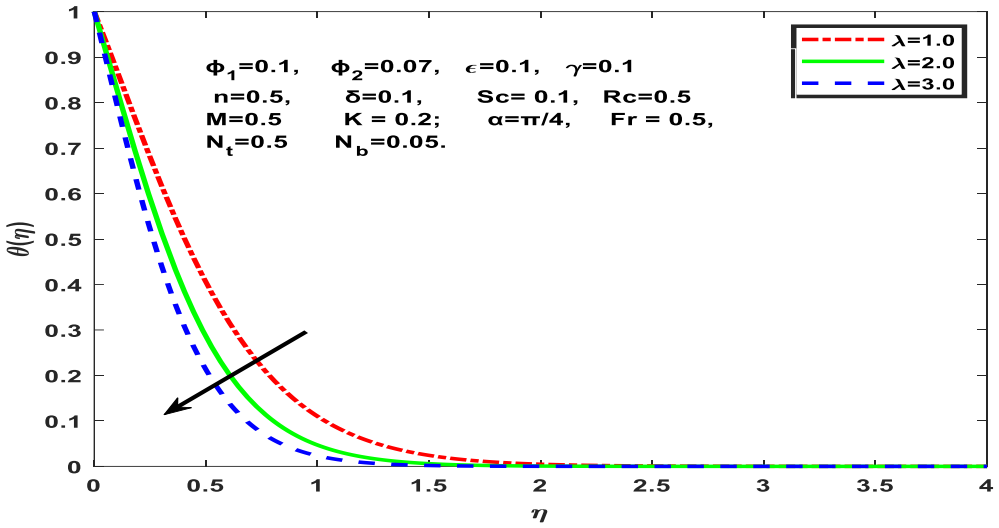

Fig. 28. Consequences of λ on Temperature θ

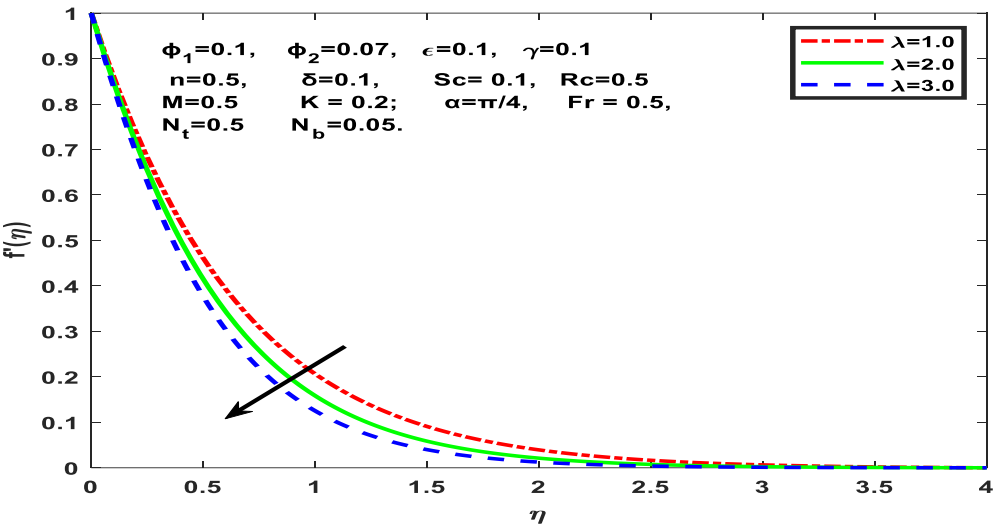

Fig. 29. Consequences of λ on Velocity f'

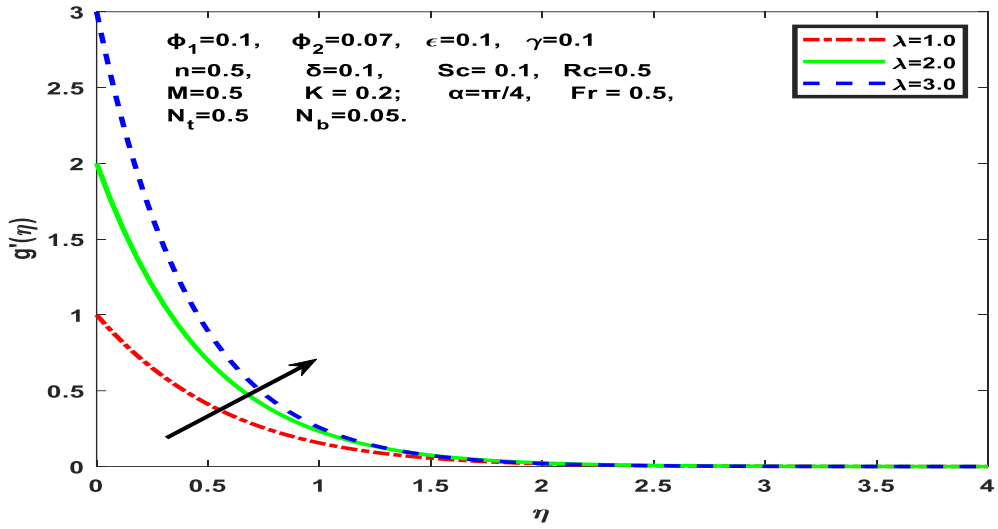

Fig. 30. Consequences of λ on Velocity g'

Figures 31-32 depicts aligned magnetic field parameter α impact on $f'(\eta)$ and$g'(\eta)$. It is noticed that $f'(\eta)$ decreasing and $g'(\eta)$ is increasing as α increases. The increment in α increases the Lorentz force by strengthening the magnetic flux, which prompts friction between the fluid surfaces and a decline in fluid velocity.

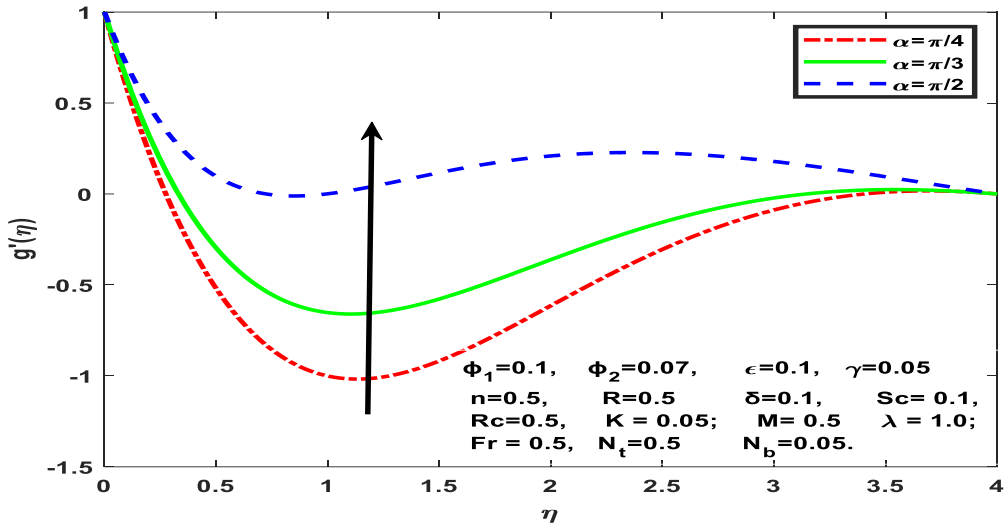

Fig. 31. Consequences of α on Velocity g'

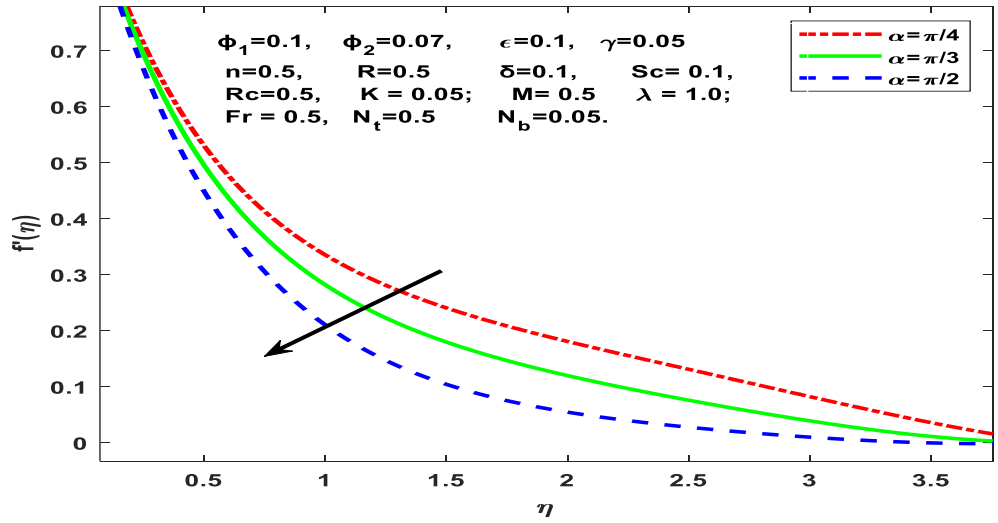

Fig. 32. Consequences of α on Velocity f'

Figures 33-36 depict Forchheimer number Fr impact on velocity distribution along x and y-axes $f'(\eta)$ and $g'(\eta)$, temparature $\theta(\eta)$ and the concentration profile $\phi(\eta)$ for $Ag - CuO/H_2O$ hybrid nanofluid. Greater Fr leads to decreases concentration $\phi(\eta)$ and velocity along both axis (x-axis and y-axis) $f'(\eta)$ and $g'(\eta)$ and increment in temperature profile $\theta(\eta)$. Physically, Increasing Fr causes a resistance to motion due to inertia; this slows things down. and $f'(\eta)$, $g'(\eta)$ and $\phi(\eta)$ decreases. The higher inertial forces and turbulence cause the hybrid nanofluid to spread out and dilute, resulting in a rise in $\theta(\eta)$.

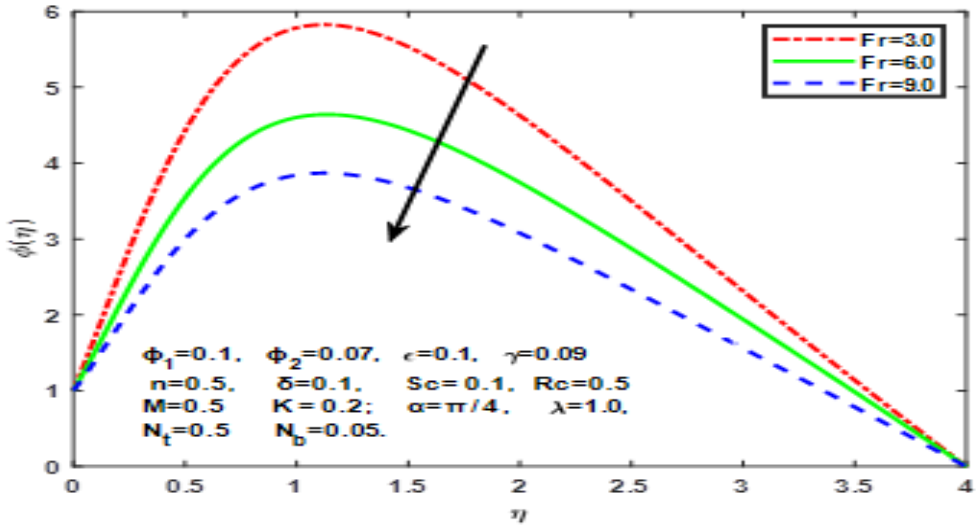

Fig. 33. Consequences of Fr on concentration Ø

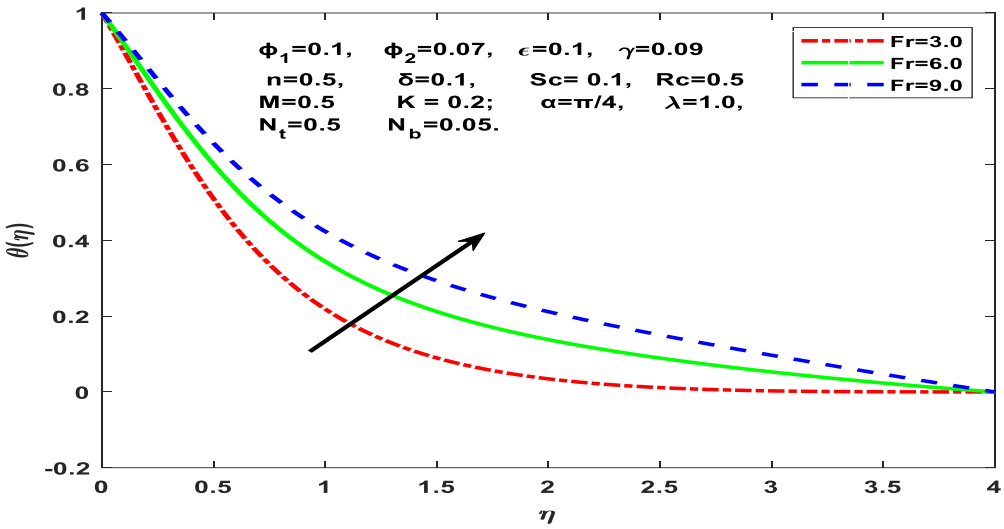

Fig. 34. Consequences of Fr on temperature Ø

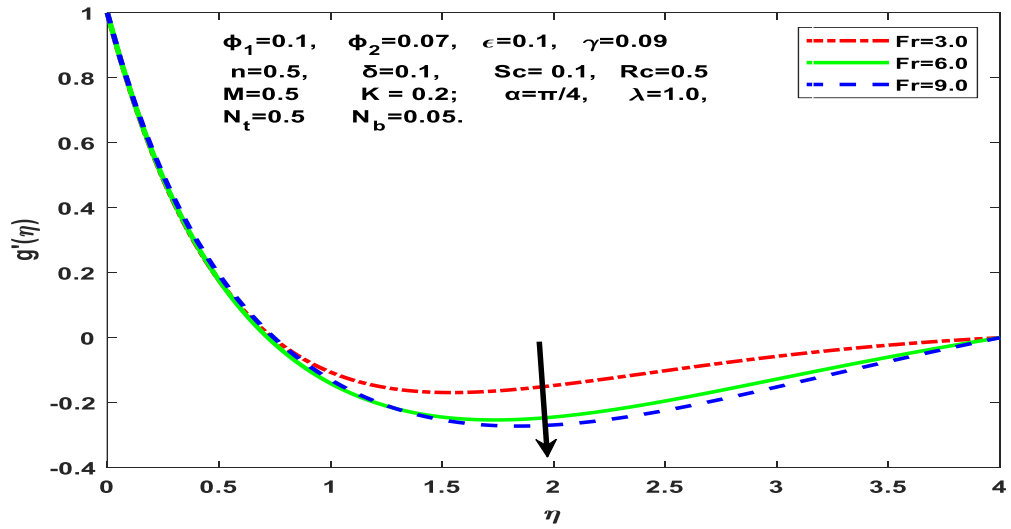

Fig. 35. Consequences of Fr on Velocity g'

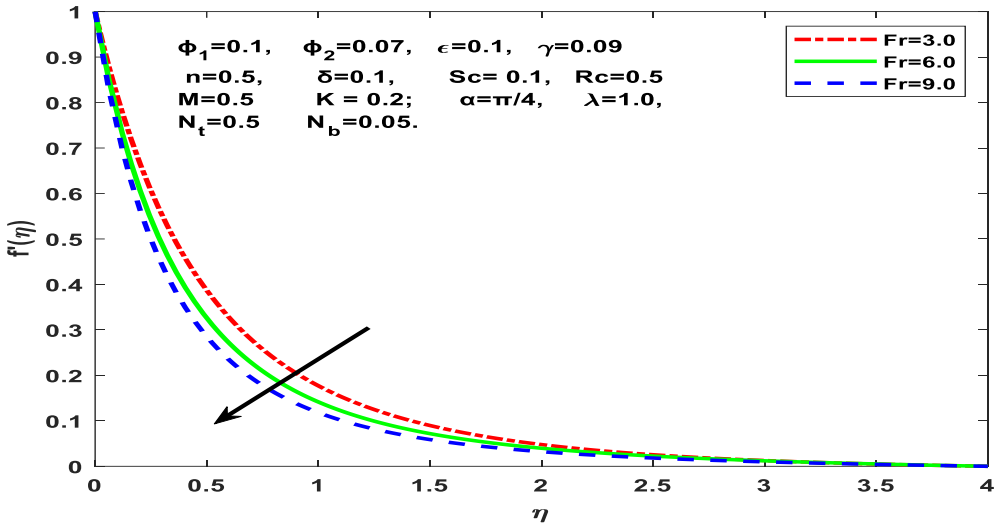

Fig. 36. Consequences of Fr on Velocity f'

The effect of the thermophoresis parameter *Nt* on the temperature and the particulate concentration profile is shown in Figures 37-38. It is evident that as *Nt* increases, temperature and quantity of fields also rise. The thermophoresis parameter is significant in the heat transmission process. When *Nt* is raised, the thermophoresis force increases, which tends to move the nanoparticles from the hot area to the cold, raising the temperature and thickening the boundary layer.

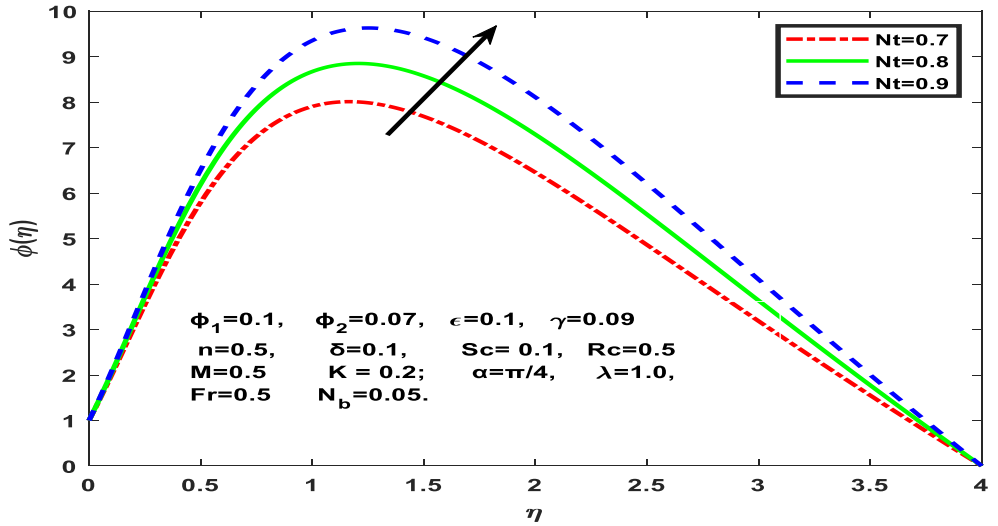

Fig. 37. Consequences of Nt on concentration ∅

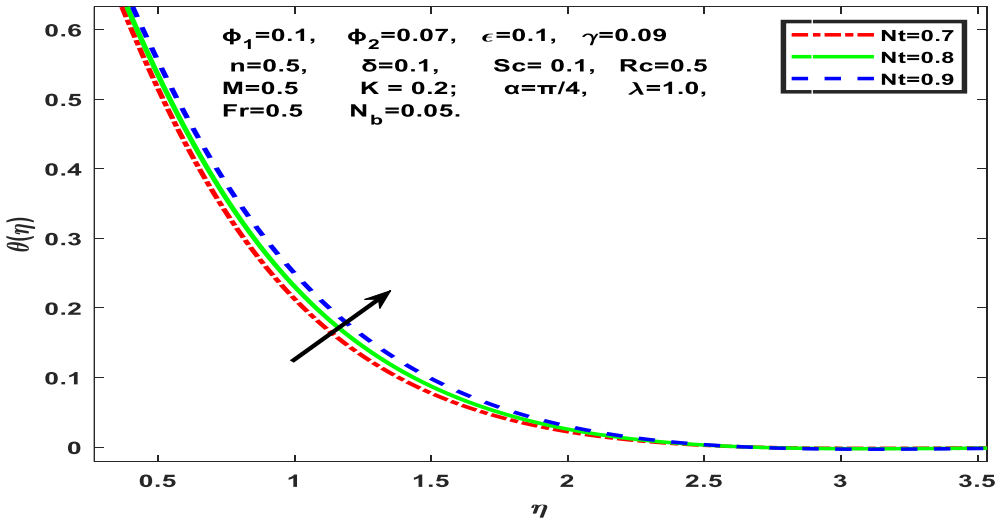

Fig. 38. Consequences of Nt on concentration θ

Figures 39-40 study the impact of the Brownian motion coefficient *Nb* on temperature and concentration levels. These results show that while an increase in *Nb* values produces a decrease in nanoparticle concentration potential, it increases temperature. When nanoparticles collide with fluid particles, Brownian motion occurs, which is the unpredictable movement of nanoparticles suspended in the fluid. When the thermophoretic effect increases, the Brownian motion effect also increases, which results in an increase in moving energy, which raises the temperature. The nanoparticles in a hybrid nanofluid are small enough to be susceptible to Brownian motion, which can improve the fluid's thermal conductivity by speeding up particle collisions and the heat transfer they cause. The viscosity and mass of the fluid can be impacted by Brownian motion, which in turn can have an effect on how the fluid flows.

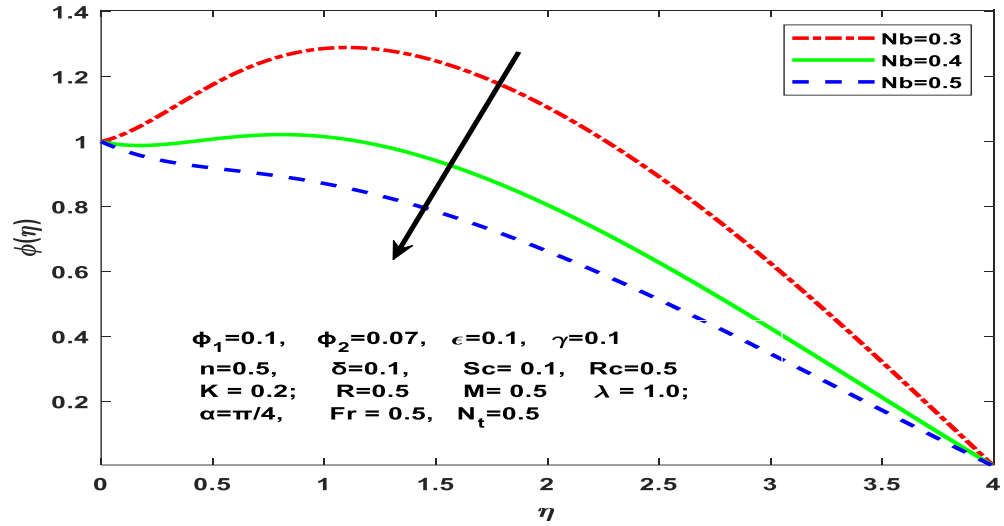

Fig. 39. Consequences of Nb on concentration $\emptyset$

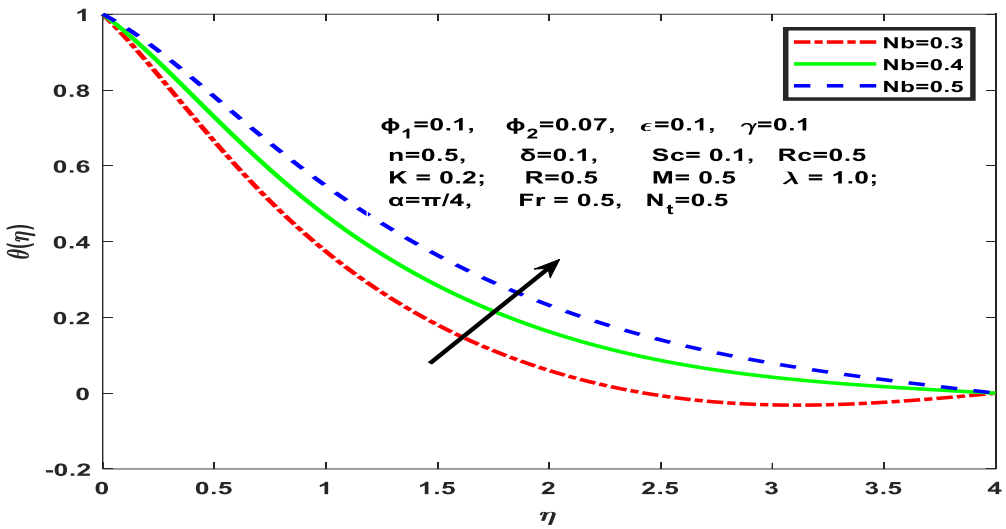

Fig. 40. Consequences of Nb on temperature θ

While thermophoresis can assist in managing the distribution and concentration of nanoparticles within the fluid, Brownian motion can improve the fluid's thermal conductivity, enhancing its capacity to transfer heat to the surrounding fluid. While calculating $-f''(0), -g''(0), -\theta'(0)$ and $-\phi'(0)$ in Tables 4 and 5, we have taken $\mathrm{Fr} = 0.5, \epsilon = 0.1, \gamma = 0.09, \mathrm{K} = 0.2, \mathrm{M} = 0.5, \alpha = \frac{\pi}{4}$, $R = 0.5$, $Sc = 0.22$, $Rc = 0.5, \lambda = 1, \mathrm{Nt} = 0.5$ and $\mathrm{Nb} = 0.05$. Keeping other parameters are same while changing one parameter. Table 3 shows the impact of skin friction in both x and y paths for $\mathrm{Fr}, \epsilon, \mathrm{K}, \mathrm{M}, \alpha, \lambda, Nt$ *and* Nb. It is noted, as the values of $\mathrm{Fr}, \mathrm{M}, \alpha$ and λ increase the skin friction in both x and y- directions increases. Down trend observed in case of K. Also, as the values of ϵ and Nb increase the skin friction increases in x-direction and decreases in y-direction, a complete opposite behaviour to this is observed for Nt.

Table 3
Influences of $-f''(0)$ and $-g''(0)$ for $\mathrm{Ag}-\mathrm{CuO}/\mathrm{H_2O}$ hybrid nanofluid

Fr	**ϵ**	**K**	**M**	**α**	**λ**	Nt	Nb	$\frac{-1}{(1-\phi_1)^{2.5}(1-\phi_2)^{2.5}}f''(0)$	$\frac{-1}{(1-\phi_1)^{2.5}(1-\phi_2)^{2.5}}g''(0)$
1.0								2.631139	2.372000
2.0								3.020498	2.399101
3.0								3.367544	2.429598
	0.02							2.266741	2.515600
	0.03							2.256224	2.682275
	0.04							2.245078	2.855430
		0.2						2.276775	2.354140
		0.3						2.223754	2.303895
		0.4						2.169571	2.252748
			1.0					2.410545	2.481684
			2.0					2.659124	2.721052
			3.0					2.887201	2.942640
				$\pi/6$				2.207120	2.288170
				$\pi/3$				2.344541	2.418623
				$\pi/2$				2.410545	2.481684
					1.05			2.290098	2.502914
					1.10			2.303308	2.654945
					1.15			2.316410	2.810159
						0.02		2.326143	3.824064
						0.03		2.326159	3.823932
						0.04		2.326184	3.823710
							0.7	2.326189	3.823668
							0.8	2.326181	3.823734
							0.9	2.326172	3.823812

Table 4 shows the impact of Nusselt and the Sherwood numbers for $\mathrm{Fr}, \epsilon, \mathrm{K}, \mathrm{M}, \alpha, \lambda, Nt, Nb$. It is noted, as the enhanced values of Fr, $\epsilon, \mathrm{M}, \alpha$ and Nb decreases both Nusselt and the Sherwood numbers, complete opposite behaviour observed in case of λ. Moreover, it is notified that the enhanced for Nt increases the Nusselt and decreases the Sherwood numbers.

Table 4
Influences of $-\theta'(0)$ and $-\phi'(0)$ for $\mathrm{Ag}-\mathrm{CuO}/\mathrm{H_2O}$ hybrid nanofluid

Fr	**ϵ**	**K**	**M**	**α**	**λ**	Nt	Nb	$-\frac{K_{hnf}}{K_f}\theta'(0)$	$-(\mathbf{1}-\boldsymbol{\phi_1})(\mathbf{1}-\boldsymbol{\phi_2})\phi'(0)$
1.0								1.173941	0.067306
2.0								1.152981	0.065592
3.0								1.134658	0.064079
	0.02							1.181197	0.067292
	0.03							1.167857	0.065457
	0.04							1.153050	0.063302
		0.2						1.193414	0.068892
		0.3						1.201205	0.069846
		0.4						1.209092	0.070814
			1.0					1.173449	0.066456
			2.0					1.135268	0.061794
			3.0					1.099131	0.057322
				$\pi/6$				1.203634	0.070144
				$\pi/3$				1.183354	0.067663
				$\pi/2$				1.173449	0.066456
					1.05			1.216094	0.069410
					1.10			1.238395	0.069854
					1.15			1.260341	0.070232
						0.02		0.692880	0.299757
						0.03		0.699791	0.290925
						0.04		0.706808	0.282026
							0.7	1.013873	0.306027
							0.8	0.935524	0.306025
							0.9	0.859479	0.306024

The values of $-f''(0)$ are comparing with Hayat and Nadeem [22] & Butt and Asif [23] and in Table 5 for various values of λ. From this present results satisfactory concordance with the current findings, Hayat and Nadeem [22], when $\phi_1 = \phi_2 = \mathrm{Fr} = \epsilon = \mathrm{K} = \mathrm{M} = \alpha = R = Sc = Rc = \lambda = 0$ and $\gamma = 0.001$.

Table 5
Comparision of $-f''(0)$ with Hayat and Nadeem [22] and Butt and Asif [23]

λ	Hayat and Nadeem [22]	Butt and Asif [23]	Present Results
0.0	1	1	1.001300
0.1	1.02137	1.020260	1.021351
0.2	1.0404	1.039495	1.040443
0.3	1.05871	1.057955	1.058703
0.4	1.07643	1.075788	1.076451
0.5	1.09364	1.093095	1.093613

5. Conclusions

This research deals 3-D, $\mathrm{Ag}-\mathrm{CuO}/\mathrm{H_2O}$ hybrid nanofluid rotating flow on a linearly stretched surface with Forchheimer number, porosity, magnetic and aligned magnetic field parameters on

velocity distributions in x and y directions, temperature and concentration profiles. In this investigation, the following conclusions are obtained.

Increased volume fractions of CuO and Ag nanoparticles in a hybrid nanofluid resulted in an increase in concentration and velocity profiles, a decrease in temperature, correspondingly, the thickness of concentration and momentum boundary layers are enhanced while thermal boundary layer thickness reduced. The hybrid nanofluid concentration decreases with greater $\phi_2, \epsilon, \mathrm{R}, \mathrm{Fr}, \mathrm{M}, \mathrm{Sc}, \mathrm{Rc}, \mathrm{Nb}$, noting that the thickness of concentration boundary layer reduced and the reversal trend is noted for the parameters $\phi_1$and Nt. The skin friction in x and y directions increases as Fr, M, α and λ increase. For ϵ and Nt it is decreasing in x direction and increasing in y direction, a complete opposite behaviour to this is observed for Nb. The Nusselt and Sherwood numbers, increases with raising values of K and λ, a complete opposite behaviour is observed for $Fr, \epsilon, \mathrm{M}, \alpha$ and Nb.

In future one may explore the various characteristics of 3-D MHD flow of hybrid nanofluid with non-linear thermal radiation, joule heating, hall and ion effects, heat and mass heat fluxes and so on are the features through modern and advanced numerical computing skills based on artificial intelligence, Machining learning and other techniques also.

Acknowledgement
This research was not funded by any grant.

References

[1] Crane, Lawrence J. "Flow past a stretching plate." *Zeitschrift für angewandte Mathematik und Physik ZAMP* 21 (1970): 645-647. https://doi.org/10.1007/BF01587695

[2] Hayat, Tanzila, S. Nadeem, and A. U. Khan. "Rotating flow of Ag-CuO/H 2 O hybrid nanofluid with radiation and partial slip boundary effects." *The European Physical Journal E* 41 (2018): 1-9. https://doi.org/10.1140/epje/i2018-11682-y

[3] Thakur, Archie, and Shilpa Sood. "Tri-Hybrid Nanofluid Flow Towards Convectively Heated Stretching Riga Plate with Variable Thickness." *Journal of Nanofluids* 12, no. 4 (2023): 1129-1140. https://doi.org/10.1166/jon.2023.1990

[4] Sreedevi, P., P. Sudarsana Reddy, and Ali Chamkha. "Heat and mass transfer analysis of unsteady hybrid nanofluid flow over a stretching sheet with thermal radiation." *SN Applied Sciences* 2, no. 7 (2020): 1222. https://doi.org/10.1007/s42452-020-3011-x

[5] Azwadi, CS Nor, and I. M. Adamu. "Turbulent force convective heat transfer of hybrid nano fluid in a circular channel with constant heat flux." *Journal of Advanced Research in Fluid Mechanics and Thermal Sciences* 19, no. 1 (2016): 1-9.

[6] Zainal, Nurul Amira, Kohilavani Naganthran, and Roslinda Nazar. "Unsteady MHD rear stagnation-point flow of a hybrid nanofluid with heat generation/absorption Effect." *Journal of Advanced Research in Fluid Mechanics and Thermal Sciences* 87, no. 1 (2021): 41-51. https://doi.org/10.37934/arfmts.87.1.4151

[7] Farooq, Umar, Madeeha Tahir, Hassan Waqas, Taseer Muhammad, Ahmad Alshehri, and Muhammad Imran. "Investigation of 3D flow of magnetized hybrid nanofluid with heat source/sink over a stretching sheet." *Scientific Reports* 12, no. 1 (2022): 12254. https://doi.org/10.1038/s41598-022-15658-w

[8] Kumbhakar, Bidyasagar, and Susmay Nandi. "Unsteady MHD radiative-dissipative flow of Cu-Al2O3/H2O hybrid nanofluid past a stretching sheet with slip and convective conditions: A regression analysis." *Mathematics and Computers in Simulation* 194 (2022): 563-587. https://doi.org/10.1016/j.matcom.2021.12.018

[9] Teh, Yuan Ying, and Adnan Ashgar. "Three dimensional MHD hybrid nanofluid Flow with rotating stretching/shrinking sheet and Joule heating." *CFD Letters* 13, no. 8 (2021): 1-19. https://doi.org/10.37934/cfdl.13.8.119

[10] Khan, Ansab Azam, Khairy Zaimi, Suliadi Firdaus Sufahani, and Mohammad Ferdows. "MHD flow and heat transfer of double stratified micropolar fluid over a vertical permeable shrinking/stretching sheet with chemical reaction and heat source." *Journal of Advanced Research in Applied Sciences and Engineering Technology* 21, no. 1 (2020): 1-14. https://doi.org/10.37934/araset.21.1.114

[11] Mohamed, Muhammad Khairul Anuar, Siti Hanani Mat Yasin, Mohd Zuki Salleh, and Hamzeh Taha Alkasasbeh. "MHD stagnation point flow and heat transfer over a stretching sheet in a blood-based casson ferrofluid with newtonian heating." *Journal of Advanced Research in Fluid Mechanics and Thermal Sciences* 82, no. 1 (2021): 1-11. https://doi.org/10.37934/arfmts.82.1.111

[12] Yashkun, Ubaidullah, Khairy Zaimi, Nor Ashikin Abu Bakar, and Mohammad Ferdows. "Nanofluid stagnation-point flow using Tiwari and Das model over a stretching/shrinking sheet with suction and slip effects." *Journal of Advanced Research in Fluid Mechanics and Thermal Sciences* 70, no. 1 (2020): 62-76. https://doi.org/10.37934/arfmts.70.1.6276

[13] Bakar, Fairul Naim Abu, and Siti Khuzaimah Soid. "MHD stagnation-point flow and heat transfer over an exponentially stretching/shrinking vertical sheet in a micropolar fluid with a Buoyancy effect." *Journal of Advanced Research in Numerical Heat Transfer* 8, no. 1 (2022): 50-55.

[14] Joshi, Navneet, Alok K. Pandey, Himanshu Upreti, and Manoj Kumar. "Mixed convection flow of magnetic hybrid nanofluid over a bidirectional porous surface with internal heat generation and a higher-order chemical reaction." *Heat transfer* 50, no. 4 (2021): 3661-3682. https://doi.org/10.1002/htj.22046

[15] Kayalvizhi, J., and A. G. Vijaya Kumar. "Entropy Analysis of EMHD Hybrid Nanofluid Stagnation Point Flow over a Porous Stretching Sheet with Melting Heat Transfer in the Presence of Thermal Radiation." *Energies* 15, no. 21 (2022): 8317. https://doi.org/10.3390/en15218317

[16] Saeed, Anwar, Wajdi Alghamdi, Safyan Mukhtar, Syed Imad Ali Shah, Poom Kumam, Taza Gul, Saleem Nasir, and Wiyada Kumam. "Darcy-Forchheimer hybrid nanofluid flow over a stretching curved surface with heat and mass transfer." *PLoS One* 16, no. 5 (2021): e0249434. https://doi.org/10.1371/journal.pone.0249434

[17] Usman, Muhammad, Sahrish Amin, and Anwar Saeed. "Magnetohydrodynamic hybrid nanofluid flow with the effect of Darcy–Forchheimer theory and slip conditions over an exponential stretchable sheet." *Advances in Mechanical Engineering* 14, no. 8 (2022): 16878132221116479. https://doi.org/10.1177/16878132221116479

[18] Haq, Izharul, Mansour F. Yassen, Mohamed E. Ghoneim, Muhammad Bilal, Aatif Ali, and Wajaree Weera. "Computational Study of MHD Darcy–Forchheimer hybrid nanofluid flow under the influence of chemical reaction and activation energy over a stretching surface." *Symmetry* 14, no. 9 (2022): 1759. https://doi.org/10.3390/sym14091759

[19] Fayyadh, Mohammed M., Rozaini Roslan, R. Kandasamy, Inas R. Ali, and Nisreen A. Hussein. "Effect of Biot Number on Convective Heat Transfer of DarcyForchheimer Nanofluid Flow over Stretched Zero Mass Flux Surface in the Presence of Magnetic Field." *Journal of Advanced Research in Fluid Mechanics and Thermal Sciences* 59, no. 1 (2019): 93-106.

[20] Ewis, Karem Mahmoud. "Analytical solution of modified Bingham fluid flow through parallel plates channel subjected to forchheimer medium and Hall current using linearized differential transformation method." *Journal of Advanced Research in Numerical Heat Transfer* 4, no. 1 (2021): 14-31.

[21] Khan, M. Riaz, Mingxia Li, Shipeng Mao, Rashid Ali, and Suliman Khan. "Comparative study on heat transfer and friction drag in the flow of various hybrid nanofluids effected by aligned magnetic field and nonlinear radiation." *Scientific Reports* 11, no. 1 (2021): 3691. https://doi.org/10.1038/s41598-021-81581-1

[22] Hayat, Tanzila, and S. Nadeem. "Heat transfer enhancement with Ag–CuO/water hybrid nanofluid." *Results in physics* 7 (2017): 2317-2324. https://doi.org/10.1016/j.rinp.2017.06.034

[23] Butt, Adnan Saeed, and Asif Ali. "Investigation of entropy generation effects in magnetohydrodynamic three-dimensional flow and heat transfer of viscous fluid over a stretching surface." *Journal of the Brazilian Society of Mechanical Sciences and Engineering* 37 (2015): 211-219. https://doi.org/10.1007/s40430-014-0163-x

[24] Abdollahi, S. A., P. Jalili, B. Jalili, H. Nourozpour, Y. Safari, P. Pasha, and D. D. Ganji. "Computer simulation of Cu: AlOOH/water in a microchannel heat sink using a porous media technique and solved by numerical analysis AGM and FEM." *Theoretical and Applied Mechanics Letters* 13, no. 3 (2023): 100432. https://doi.org/10.1016/j.taml.2023.100432

[25] Jalili, Bahram, Narges Aghaee, Payam Jalili, and Davood Domiri Ganji. "Novel usage of the curved rectangular fin on the heat transfer of a double-pipe heat exchanger with a nanofluid." *Case Studies in Thermal Engineering* 35 (2022): 102086. https://doi.org/10.1016/j.csite.2022.102086

[26] Jalili, Bahram, Amirhossein Rezaeian, Payam Jalili, Davood Domeri Ganji, and Yasir Khan. "Squeezing flow of Casson fluid between two circular plates under the impact of solar radiation." *ZAMM-Journal of Applied Mathematics and Mechanics/Zeitschrift für Angewandte Mathematik und Mechanik* (2023): e202200455. https://doi.org/10.1002/zamm.202200455

[27] Jalili, Bahram, Hassan Roshani, Payam Jalili, Mohammad Jalili, Pooya Pasha, and Davood Domiri Ganji. "The magnetohydrodynamic flow of viscous fluid and heat transfer examination between permeable disks by AGM and FEM." *Case Studies in Thermal Engineering* 45 (2023): 102961. https://doi.org/10.1016/j.csite.2023.102961

[28] Jalili, Bahram, Amirhossein Rezaeian, Payam Jalili, Fathollah Ommi, and Davood Domiri Ganji. "Numerical modeling of magnetic field impact on the thermal behavior of a microchannel heat sink." *Case Studies in Thermal Engineering* 45 (2023): 102944. https://doi.org/10.1016/j.csite.2023.102944

[29] Jalili, Bahram, Payam Jalili, Sina Sadighi, and Davood Domiri Ganji. "Effect of magnetic and boundary parameters on flow characteristics analysis of micropolar ferrofluid through the shrinking sheet with effective thermal conductivity." *Chinese Journal of Physics* 71 (2021): 136-150. https://doi.org/10.1016/j.cjph.2020.02.034

[30] Jalili, Bahram, Sina Sadighi, Payam Jalili, and Davood Domiri Ganji. "Characteristics of ferrofluid flow over a stretching sheet with suction and injection." *Case Studies in Thermal Engineering* 14 (2019): 100470. https://doi.org/10.1016/j.csite.2019.100470